Conjugate Heat Transfer: Some Fundamentals and Recent Progress

(Chapter 2, Advances in Heat Transfer, Vol.55, Elsevier, May 2023)

L. He

Department of Engineering Science,
University of Oxford, Oxford, UK
(email: Li.He@eng.ox.ac.uk)

Abstract

For convective heat transfer, the fluid-domain based decoupled approach has been well established and widely applied for a long time. In this approach, the convective heat transfer coefficient is solved from the perspective of the fluid, without consideration of conductive heat transfer within the solid object. Fluid-solid coupled conjugate heat transfer (CHT), a seemingly more complete approach with higher fidelity, though computationally more involved, has also been continuously developed and applied in past decades. With CHT, the heat transfer at the interface between the fluid and the solid is determined holistically, with both internal conduction and external convection combined together. It is rather noteworthy however that there is a lack of discussion on the role of the CHT: when should CHT be applied and why and how should it be applied? These issues seem to be intrinsically linked to other questions such as when, why and how would the convectional fluid-only decoupled approach be limited? In this chapter, we will start with a brief introduction to the general background of the conventional heat transfer coefficient based decoupled approach and its underlying wisdom. Then we will carry out a more systematic analysis and discussion on the theoretical bases underpinning the conventional approach. Particular attention will be paid to two contrasting theoretical regimes: a linear fluid flow system and a nonlinear one. It is shown that the validity and applicability of the conventional HTC based approach will be challenged in the two regimes in different ways respectively, also with different implications within the context of CHT and beyond. Then we will look at the specific physical and numerical modelling challenges arising from the time scale disparity, and how it may impact our solution capability for time-dependent CHT problems. Some recent progress will be presented in addressing the challenging issues with a new multiscale modelling strategy, particularly for CHT methods with scale-resolving Large Eddy Simulation (LES) turbulent flow solutions.

Keywords: Convective Heat Transfer, Heat Transfer Coefficient, Conjugate Heat Transfer, Influence Coefficient, Fluid-solid Interface, Fourier method, Multiscale, Large Eddy Simulation.

1. Background and Issues of Interest

Prediction of convective heat transfer is relevant to a wide range of engineering problems. For instance, consider the performance, thermal mechanical integrity and lifespan of hot-end components of gas turbines/aero-engines. Thermal analysis is necessarily required as part of a turbomachinery design system. It is normally the case that design methods and tools are much more well-established for nominal steady (or periodically unsteady) states than those for dynamic transient processes. Increasingly, adequate predictions of transient thermal characteristics during start-up, shut-down and load-changing conditions of power generation operations for steam turbines, gas turbines and aero-engines are of great interest. In particular, the growing renewable energy market share requires more flexible steam turbine operations. In order to design a steam turbine to operate reliably for flexible operations, designers need to understand and predict dynamic thermal characteristics of steam turbine components during a transient process. Similarly, for gas turbines, the thermal fatigue life span is also strongly dependent on the predictability of transient thermal behaviour of the hot components during an operation cycle. Turbine thermal dynamic characteristics are strongly influenced by various convective heat transfer phenomena. Analysis and prediction of the problems related to natural convection are more challenging with less well-established theories, methods, or even empirical correlations, compared to their forced convection counterparts. As natural convection as well as mixed natural and forced convection can be strongly influential for a large part of a flexible operation process, the emerging practical requirement for flexible operations has also motived recent active developments of advanced aerothermal modelling and prediction methods.

In general, aerothermal design and analysis for convective heat transfer face challenges arising from the difference between a R&D environment in which reasonably detailed and accurate data (typically at a low speed and low temperature condition) can be acquired and a realistic operational environment (typically at a high speed and/or high temperature condition). The development of advanced modelling and simulations methods will help address the challenges. But newly advanced models and simulation methods also need to be validated adequately, and these validations need to be made against well-conditioned and detailed experimental measurements in good quality, which again tend to be available only at low temperature and low speed conditions. Therefore, aerothermal designs and analyses tend to be linked to our capability of scaling the relevant parameters from different flow speeds and/or temperature conditions. Dimensional analysis forms the basis for the scaling for convective heat transfer parameters, typically relating the Nusselt number Nu to the Reynolds number Re, the Mach number M, and the Prandtl number

Pr, (E.q.1-1a) or for a low speed incompressible flow where the Mach number does not feature (Eq.1-1b), e.g. [1].

$$Nu = f(Re, M, Pr) \quad (1\text{-}1a)$$

$$Nu = f(Re, Pr) \quad (1\text{-}1b)$$

The Nusselt number represents the ratio of convection to diffusion. Effectively Nu is a non-dimensional heat transfer coefficient, normalised by a characteristic length and fluid thermal conductivity.

$$Nu = hL/k \quad (1\text{-}2)$$

where h is heat transfer coefficient (HTC) as formulated in Newton's Law of Cooling [1]:

$$q = h(T_f - T_w) \quad (1\text{-}3)$$

where q is a surface heat flux, T_f and T_w are the temperatures of the fluid and the solid wall, respectively. Clearly, of the four parameters in Newton's law of cooling, heat flux q and wall temperature T_w are physical parameters, which are directly measurable (computable). For the other two, the HTC and the 'fluid driving temperature' T_f, different definitions and interpretations exist. Therefore both HTC and T_f are essentially 'open parameters', however are also intrinsically linked by being subject to the basic constraint that for given q and T_w, any combinations of h and T_f (regardless of how they are 'chosen') will have to satisfy Eqs. 1-3. In the way, it should be anticipated that uncertainty in HTC tends to be intrinsically linked to uncertainty in T_f.

Generally speaking, the focal point in the convective heart transfer community tends to be the HTC, as reflected by the long-term quest for consistently defined and practically workable 'invariant descriptors' for convective heat transfer (Moffatt [2]). In this context, an 'invariant descriptor' means its independence of the wall heat transfer (thus T_w). A basic assumption of an HTC based method is that convective heat transfer is predominantly (if not completely) determined by fluid mechanics/aerodynamics with negligible feedback from heat transfer at the fluid-solid interface. This is consistent with the linear relation between heat flux and wall temperature, as implied in Newton's law of cooling. The conventional wisdom is also consistent with the expectation of the HTC (in one form or another) being an 'invariant descriptor' completely determined by the flow, independent of the wall temperature.

For practical applications of thermal fatigue life designs and durability predictions for heating/cooling sensitive components, temperature distributions in the solid are needed. Nu is typically used to scale HTC from one condition to another. With an HTC based approach, one can adopt a decoupled procedure. An HTC distribution over a solid surface can be obtained first based on either an empirical correlation (typically based on Nusselt number for scaling to different geometrical and working conditions), an experimental measurement, or a numerical simulation in the fluid domain only. It can then be used to solve a conduction equation for solid domain only with convective boundary conditions with the HTC and fluid temperature commonly taken as invariant to the solid wall temperature. This approach is in line with the basic assumption that the wall heat transfer does not affect fluid dynamics which dictates convective heat transfer.

In the past few decades, development of computational fluids dynamics (CFD) has greatly enhanced capabilities in predicting detailed flow field features and also enhanced the prediction of detailed HTC distributions for complex practical configurations. On the other hand, fluid-solid coupled Conjugate Heat Transfer (CHT) methodologies and working methods have also been extensively developed. In a CHT, there is no HTC needed, and solid (as well as fluid) temperatures will be part of the CHT solution. From a design perspective, HTC/Nu distributions in data sets or in correlations would conveniently enable a fast-iterative design exercise. From a solution accuracy perspective, CHT should be of a higher modelling fidelity, but a fluid-solid coupled solution would certainly be more costly. Also, a CHT solution does not lend itself easily to a form readily useable for fast design iterations, e.g. by the HTC scaling through Nu correlations.

A general issue of interest, which has been rarely discussed (somewhat surprisingly), is when should a CHT approach start, and when should an HTC approach be left off? Given the lack of the discussion in the literature on this issue, it is felt necessarily beneficial that we take a more fundamental look at some theoretical bases which may underpin the conventional HTC based approach. There are two related questions: a) what is the theoretically formal basis for the HTC (or the likes of ‘invariant descriptor’)? b) what is the applicability of an HTC based approach? Here we would like to approach these questions in terms of flow regimes (incompressible vs. compressible) and their aerothermal interactive nature (linear vs. nonlinear).

Clear understanding of the basis for the HTC-based approach and the implications for the applicability should motivate the development and application of CHT. However, CHT methods also face their own challenges, particularly when developed for analysing transient CHT problems chiefly due to the time-scale disparity between fluid and solid. These issues should be addressed

in developing advanced CHT methods particularly in conjunction with high-fidelity scale-resolving turbulence flow (LES) solvers.

The following sections are organised in order to address these rather fundamental questions as raised above so that a case for CHT can be made more clearly. The issues and challenges of CHT are also discussed and some recent progress aimed at addressing them will be presented. We will first look at the theoretical basis for the conventional HTC based approach, then we will examine some situations where the basis may be questioned, backed up by some examples to serve as the motivating cases for CHT. The challenges for CHT in terms of the time scale disparity will then be discussed. In particular, the disparity manifested markedly in transient CHT for long time scales for turbine flexible power generation operations at one end, and for small time scales associated with scale-resolving (LES) turbulence solutions based CHT at the other end of the spectrum, will be addressed. Some new multiscale frameworks and methodologies that have been recently developed will be presented.

2. Linear Flow Energy Equation and Heat Transfer 'Invariant Descriptor'

Given the long-standing development and application of the HTC based approach, it would be useful to take a systematic look at the relevant theoretical basis. At the heart of the matter is how the fluid thermal (temperature) field and the momentum (velocity) field are inter-linked. We will start with the flow governing equations in the two basic settings of general interest, compressible flow and incompressible flow. We will then be able to see how the temperature field would behave passively and linearly in an incompressible flow and how the two fields may interact mutually nonlinearly in a compressible flow setting. Then, we shall have a clearer picture regarding where and how the HTC as well as other possible 'invariant descriptors' for convective heat transfer should fit in with a reasonably justifiable underpinning.

2.1 Compressible Flow vs. Incompressible Flow Systems

Consider an unsteady compressible aerodynamic flow field governed by the conservation laws for mass, momentum and energy in three dimensions (x, y, z) with the corresponding velocity components u, v, w; density ρ; pressure P; and temperature T. The corresponding equation system can be written in a compact form for the lumped flux residual R. Now we consider the two regimes: first a compressible flow, then an incompressible one.

Compressible Flow:

Mass Continuity: $\frac{\partial \rho}{\partial t} - R_{mass}(u, v, w, \rho) = 0$

x momentum: $\frac{\partial \rho u}{\partial t} - R_{fx}(u, v, w, \rho, P, T) = 0$

y momentum: $\frac{\partial \rho v}{\partial t} - R_{fy}(u, v, w, \rho, P, T) = 0$

z momentum: $\frac{\partial \rho w}{\partial t} - R_{fz}(u, v, w, \rho, P, T) = 0$

Energy: $\frac{\partial \rho e}{\partial t} - R_{energy}(u, v, w, \rho, P, T) = 0$

(2-1)

where internal energy e is a function of other flow variables. Subscripts 'fx', 'fy', fz' denote the momentum in x, y, z respectively. With the equation of state, we have a closed system with six equations for six flow variables (u, v, w, ρ, P, T). All equations are closely coupled.

Then, consider an incompressible flow with a constant density and constant fluid properties.

Incompressible Flow:

Mass Continuity: $S_{mass}(u, v, w,) = 0$

x momentum: $\frac{\partial u}{\partial t} - S_{fx}(u, v, w, P) = 0$

y momentum: $\frac{\partial v}{\partial t} - S_{fy}(u, v, w, P) = 0$

z momentum: $\frac{\partial w}{\partial t} - S_{fz}(u, v, w, P) = 0$

Energy: $\frac{\partial T}{\partial t} - S_{energy}(u, v, w, P, T) = 0$

(2-2)

We can see that for an incompressible flow, the momentum (velocity and pressure) fields (u, v, w, P), can now be solved completely by only solving the mass continuity and momentum equations. So, the continuity and momentum equations now stand on their own and are decoupled from the energy equation. The energy equation is redundant as far as solving the momentum field is concerned, but the solution to the energy equation depends on the solution of the continuity and momentum equations. Consequently, we have:

i) The momentum field can be solved first before solving the energy equation. In this way we can say that the fluid momentum plays an active role while the energy field is completely passive and cannot influence the momentum field at all.

ii) Once the momentum field is solved independently of the fluid temperature, the energy equation becomes linear with constant coefficients which are simply functions of the already known velocities and pressure (u, v, w, P).

iii) It should be added that the linearity of the energy equation in an incompressible flow should not be confused with the nonlinear capability of an incompressible flow model in solving turbulence, e.g. in the scale-resolving LES. A nonlinear and unsteady turbulent flow field is still solved independently without coupling with the energy equation. The solved turbulence fluctuating field does affect the temperature thermal field transport, e.g. by impacting on thermal mixing with different values and distributions of the effective 'turbulent Prandtl number' (e.g. Ling et al [3], Milani, et al [4]). But the fundamentals remain unchanged, the energy equation is linear, and the temperature field is passively driven by the solved flow field.

2.2 Incompressible Flow: HTC and Wall Temperature Invariant Descriptor

We now examine further the passive and linear energy equation in an incompressible flow to establish a more direct link to the applicability of the HTC based approach in the form of Newton's law of cooling. For a simpler form of presentation, we express the flow variables for an incompressible flow in vector form $\boldsymbol{U}$ = (u, v, w, P)^T. After the flow momentum field is solved independently, $\boldsymbol{U}$ is known. The linear energy equation can be expressed as:

$$\frac{\partial T}{\partial t} - L(\boldsymbol{U}, T) = 0 \qquad (2\text{-}3)$$

where L denotes a linear operator for temperature T as the variable with the given (known) $\boldsymbol{U}$ field. Consider a steady state fluid temperature field subject to wall temperature T_w on a solid boundary and a reference temperature T_{ref}. A temperature response $\delta T = T - T_{ref}$ at any point within the 3-D fluid domain will be proportional to its originating boundary disturbance over a wall segment of area δA at a wall temperature perturbation $\delta T_w = T_w - T_{ref}$.

$$\delta T = C(\boldsymbol{U})\delta T_w \delta A \qquad (2\text{-}4)$$

where $C(\boldsymbol{U})$ is a spatially varying coefficient dependent only on the already-solved fluid momentum field $\boldsymbol{U}$ and thus is a constant of proportionality between the response δT and its

source disturbance δT_w per unit area ($\delta A = 1$). The total temperature response to all wall temperature disturbances from the entire solid boundary of area *A* can thus be obtained by summing up the contributing influences from all boundary points (each with its differential area *dA*) respectively, through a boundary integration.

$$\left(T - T_{ref}\right) = \oint_0^A C(\boldsymbol{U})\left(T_w - T_{ref}\right)dA \tag{2-5}$$

It should be reminded that $C(\boldsymbol{U})$ is a function of the known momentum field only. Thus, the integrand is effectively the local wall temperature disturbance weighted by the spatially variant but T_w invariant coefficient. Consider the fluid temperature distribution near the solid wall. Differentiate the above (Eq. 2-5) with respect to the wall normal distance *n*, and multiply it by a constant fluid thermal conductivity *k.*

$$k\frac{\partial T}{\partial n} = \oint_0^A g(\boldsymbol{U})\left(T_w - T_{ref}\right)dA \tag{2-6}$$

where $g(\boldsymbol{U}) = k\frac{\partial C(\boldsymbol{U})}{\partial n}$. When working out the wall heat flux ($k\frac{\partial T}{\partial n}$) at any point of interest, the term $g(\boldsymbol{U})$ can be interpreted physically as the influence of a unit wall temperature disturbance per unit wall area (when $\left(T_w - T_{ref}\right) = 1$ and $dA = 1$).

Dimensionally in SI units, $g(\boldsymbol{U})$ has units of $W/m^{-4}K^{-1}$. If one thinks of a link between $g(\boldsymbol{U})$ and HTC, the units can be simply rewritten as $(W/m^2/K)/ m^2$. The group in the numerator has the units of HTC. Thus $g(\boldsymbol{U})$ can be interpreted as the local influence per unit wall boundary area on an equivalent HTC at a point of interest.

The boundary integration (Eq. 2-6) means that the total influence on the heat flux at the point of interest needs to be summed up for all differential boundary elements over the entire wall boundary surface *A*, by superposition for the linear system. As such, $g(\boldsymbol{U})$ can be labelled as a local Influence Coefficient (IC) for a boundary point subject to a non-unit wall temperature disturbance on a non-unit area. This should be how $g(\boldsymbol{U})$ is interpreted physically for wall bounded convective heat transfer. Mathematically, $g(\boldsymbol{U})$ is Green's function linking a field response specifically to a boundary perturbation for a linear system as it is generally defined.

2.2.1 Isothermal Wall (Tw = constant)

For an isothermal wall case (T_w = const everywhere on the entire solid boundary), we then have,

$$q = \left(T_w - T_{ref}\right)\oint g(\boldsymbol{U})dA \tag{2-7}$$

The key point is that the boundary integration depends only on a known momentum field $\boldsymbol{U}$, and is completely independent of the now uniform wall temperature disturbance in this case. If we denote the integration over the wall boundary surface simply as h($\boldsymbol{U}$), we then have

$$h(\boldsymbol{U}) = -\oint g(\boldsymbol{U}) dA \tag{2-8}$$

Regardless of how the influence coefficient/Green function $g(\boldsymbol{U})$ is actually distributed (in a known form or not), the most relevant takeaway from Eq. 2-8 is that h only depends on the already independently solved flow field. We then reach the form of Newton's law of cooling:

$$q = h(\boldsymbol{U}) \left(T_{ref} - T_w\right) \tag{2-9}$$

The reference temperature, which seems to be arbitrarily introduced, will now also have to satisfy a basic physical constraint: the heat flux needs to diminish to zero (adiabatic) when the wall temperature disturbance $\left(T_w - T_{ref}\right)$ becomes zero. Thus, T_{ref} needs to be the adiabatic wall temperature T_{ad} for this physical consistency. Also noted is that the assumption of the constant wall temperature perturbation in conjunction of the isothermal wall would mean that T_{ad} needs to be constant over the entire boundary for deriving Eq.2-8. Furthermore, for an incompressible flow, the internal heat dissipation across a boundary layer tends to be negligible, thus the freestream/inlet stagnation temperature can be simply taken as T_{ad}. On a $T_w - q$ diagram (Fig.2-1), h (HTC) is a constant, and thus the slope of a straight line of q variation with T_w. T_{ad} as the fluid driving temperature can also be graphically interpreted easily and consistently as shown in Fig. 2-1.

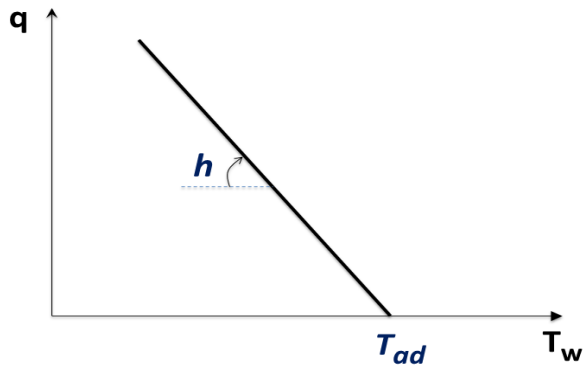

Fig. 2-1 q-T_w variation for an isothermal wall-bounded incompressible flow

Therefore, for an incompressible flow bounded by an isothermal wall, we see that the exact form of the Newton's law of cooling can be established. The corresponding heat transfer coefficient is an invariant descriptor of the heat transfer in the sense:

1) HTC is independent of the wall temperature.
2) HTC is fixed by the independently solved flow momentum field.
3) Correspondingly, the wall heat transfer and the temperature thermal field are uncoupled from and passively determined by the velocity and pressure field.

The key to the above is that the local wall temperature disturbance is the same for the entire wall boundary. Because of this, the sum of the influence (the local temperature disturbance weighted by the local influence coefficient) for each and every element of the entire wall boundary simply becomes the constant temperature disturbance weighted by the sum of the influence coefficients. Under this condition, the HTC in the form of Newton's law of cooling is indeed a T_w-invariant descriptor of convective heat transfer. In addition, the fluid driving temperature T_{ad} also effectively becomes T_w invariant for this case.

2.2.2 Non-isothermal Wall ($T_w \neq$ constant)

When the wall temperature varies on a solid boundary, the wall heat flux at a point of interest 'J' will be influenced by all local wall temperature disturbances weighted by corresponding local influence coefficients from all boundary locations. In this case, we seek a numerical or experimental solution, thus a discrete form of the equation is useful. The equivalent discrete form of the general integral expression (Eq. 2-6) for the heat flux at point *J* subject to a solid wall boundary with a total of N_w discrete wall surface elements is:

$$q_J = \sum_{i=1}^{N_w} g_{i,J}(\boldsymbol{U})\Delta T_{w_i}\Delta A_i \qquad (2\text{-}9)$$

$g_{i,J}(\boldsymbol{U})$ is the influence coefficient of boundary element '*i*' with regard to the heat flux q_J of point '*J*'. Physically, $g_{i,J}$ represents the specific influence (per unit temperature disturbance per unit area) from wall boundary element *i* of area ΔA_i .

It is recognised that an alternative and more compact form (Eq. 2-10), developed by Hacker & Eaton [5], Eaton [6], is often used.

$$q_j = \sum G_{i,j}(\boldsymbol{U})\Delta T_{w_i} \qquad (2\text{-}10)$$

where $G_{ij}(\boldsymbol{U})$ is called 'Discrete Green's Function'. $G_{i,j}(\boldsymbol{U})$ represents the specific influence per unit wall temperature disturbance from boundary element 'i'. The area of the discrete element ΔA_i is already included in $G_{i,j}$.

For a given computational or experimental partition of a solid boundary, Eq. 2-9 is equivalent to Eq. 2-10, when we take into account the factor of discrete boundary element area ΔA. Nevertheless, Eq. 2-9 is the direct discrete form of the integral equation (Eq.2-6) in which g is the Green's function as generally and formally defined. Correspondingly, $g_{i,J}$ is the direct discrete form of Green's function g. Another observation is that the normalization of $g_{i,J}(\boldsymbol{U})$ with respect to boundary area should make it more transferable to other similar configurations with different boundary partitions, should it be needed. Physically, $g_{i,J}$is effectively the Influence Coefficient (IC) of boundary point *i* with respect to heat flux at boundary point *J*. Thus, 'Influence Coefficient' may be a more suitable term for physical understanding.

Regardless of exact forms and definitions, it is emphasized that $g_{i,J}(\boldsymbol{U})$ is the function of the known flow field solution $\boldsymbol{U}$. Because $\boldsymbol{U}$ is independent of temperature (in the field or on the wall boundary), the influence coefficient $g_{i,J}$ (or 'discrete Green's function' $G_{i,j}$, Eq.2-10) is thus a wall-temperature 'invariant descriptor'. The summation form of Eq. 2-9 means that for a non-isothermal wall case, heat flux at any point on a wall should be influenced by other points on the wall. We now consider two relevant scenarios to help elaborate on what it means and implies.

Consider first a fluid-domain-only case (Fig. 2-2). For a wall bounded flow (boundary layer), the dominant transport mechanism is flow convection. In this case, flow field will remain unaffected by wall heat transfer for the given passive temperature field governed by the linear energy equation. A fluid element near the wall surface will experience a temperature change by the wall heat transfer. Thus, for this linear energy equation system, the dominant upstream convection will manifest itself in terms of the changed fluid temperature, which will impact on downstream fluid temperature by convection. Thermal diffusion in the wall normal and lateral directions tend to be far less significant. It follows then, when we consider the heat flux at the point of interest *J*, it will be subject to predominantly the convective influences from upstream locations. In other words, the affected fluid temperature is advected downstream passively at the local fluid velocity. The heating/cooling of the surface elements upstream of point *J* (including that at point *J* itself) will thus be able to influence the fluid driving temperature (and thus the heat flux) at *J*, whilst those downstream of point *J* will not. Consequently, only the upstream influence coefficients are needed, as shown in Fig. 2.2.

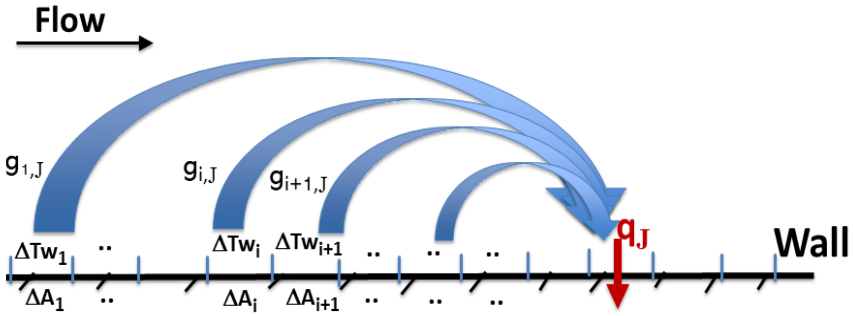

Figure 2-2 Influence on point 'J' from other boundary points (Fluid-domain only)

(Upstream Convected Cooling/Heating 'History Effect')

The discussion for a fluid-domain-only case clearly highlights the relevance of the upstream convective ('history') effect on the fluid temperature field. Here the 'history' means the accumulated upstream heating/cooling manifested in changing the fluid temperature at the point of interest, J (Fig.2-2). For this linear system, each discrete wall boundary element can exert its own influence on the point of interest *J* independently, and the total effects of all upstream boundary elements on the point can be simply summed.

However, there is a quite different picture for a fluid-solid coupled domain (Fig. 2-3). The wall surface is no longer an external boundary for the coupled domain. We can then see that those wall elements downstream of point *J* can actually influence point *J* by influencing all upstream points through thermal diffusion/conduction in the solid domain. In fact, any point on the wall surface may influence all solid boundary points, and also be influenced by all boundary points. Thus, for a fluid-domain only setting, the influences from all wall elements on the wall flux at a particular point of interest would be at best incomplete, unless those influences through the solid conduction are credibly deemed to be negligible.

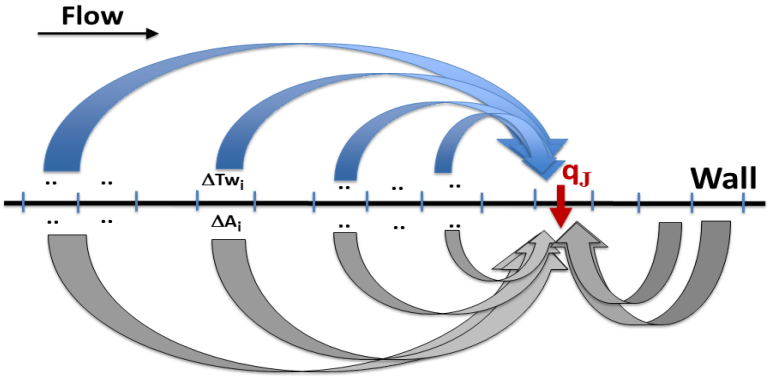

Figure 2-3 Influence on point 'J' from other boundary points (Fluid-Solid Domain)

(Upstream Convection and Up/Downstream Conduction)

An overall observation is that the linear energy equation decoupled from the mass and momentum equations in an incompressible flow can provide a basic underpinning for the existence of wall temperature-invariant descriptors for heat flux. Under an isothermal wall (uniform T_w) condition, the exact form of Newton's law of cooling can be obtained, where HTC is a T_w invariant descriptor. Also, the adiabatic wall temperature is the fluid driving temperature.

For a more general non-isothermal case, the heat flux at a solid surface point will be subject to summed influences from all solid surface points. A temperature-invariant descriptor can still be formulated in terms of the influence coefficient (the discrete form of Green's function or 'discrete Green's function'), but determining them with adequate accuracy is challenging (e.g. Anderson and Moffat [7], Batchelder and Eaton [8], Booten and Eaton [9], Mukerji and Eaton [10]).

Particular attention is paid to a fluid-domain-only setup, the common approach for convective analysis. The influence coefficients/discrete Green functions obtained for a fluid-domain only case will most likely capture only the upstream heating/cooling influences due to fluid convection. In contrast, the thermal diffusion in a solid domain propagates temperature disturbances from any wall boundary point to all other wall boundary points. Thus, the solid conduction provides an extra path to enable a downstream point on the solid wall boundary to influence all upstream points. This means that for general non-isothermal cases, even for an incompressible flow, a fluid-solid coupled conjugate heat transfer (CHT) analysis may be needed in general. CHT may also be relevant in finding a more complete set of the local influence coefficients/discrete Green's functions as wall temperature-invariant descriptors for situations where a linear and passive temperature field may be assumed, e.g. Hoffman and Eaton [11], Andreoli et al [12], Saavedra et al [13].

3. Nonlinear Aerothermal Interaction: 'Feedback' of Heat Transfer on Flow

3.1 Impact of Active Thermal Field: Heat Transfer related 'Compressibility'

Given the previous discussions on the linear energy equation and the related underpinning for the conventional HTC based approach, it is important to be able to judge when each method is most applicable and when compressibility effects must be included. From an aerodynamics perspective, one may safely assume an incompressible flow for a low speed aerodynamic flow with Mach number less than ~ 0.3. The following examples however indicate that the situation may become very different once heat transfer is introduced. The thermal condition relative to an adiabatic case can be simply expressed in terms of the temperature ratio (*TR*), which is the wall temperature normalised by the inlet flow stagnation temperature T_{01}.

$$TR=T_w/T_{01} \quad (3\text{-}1)$$

Consider a turbine blade operating at a low-speed flow condition, Mach number ~0.3. The blade surface is prescribed with a constant wall temperature. The cases are all isothermal, and *TR* is a constant for all parts of blade wall surface for each case. The first case is a baseline case, where the adiabatic condition is applied to the solid wall surface, no wall temperature needs to be specified in this case, but the fluid temperature is roughly the same as the inlet total temperature, thus $TR \approx 1$. The density contour plot is shown in Fig. 3-1a. We can see that the density field remains more or less constant with the maximum density variation in the range of smaller than 5% of the inlet density value ($\Delta\rho_{max}/\rho_1<5\%$).

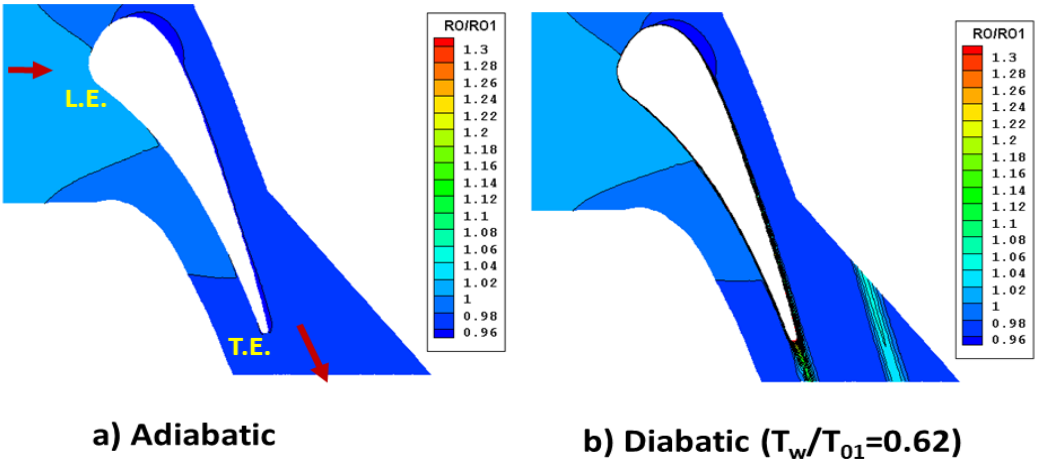

Figure 3-1 Density variation (ρ/ρ_1) around turbine blade in low speed flow (Mach ≈ 0.3)

Next, we introduce heat transfer at the same low-speed flow condition (M~0.3). The inlet total temperature is also taken to be the same (thus the inlet Reynolds number remains the same). Given typical hot gas and solid surface temperatures for high-pressure turbines, we take a wall/inflow temperature ratio, *TR*=0.62. The results for this scenario are shown in Fig. 3-1b. We now see a very distinctive density boundary layer around the solid surface with a much larger range of variation ($\Delta\rho_{max}/\rho_1$ ~ 60%). The near-wall flow region is where the key aerothermal performances (flow loss and heat transfer characteristics) are critically influenced in general. The near wall region is also where the key turbulence behaviour and its impact on friction drag and convective heat transfer are all closely relevant.

In terms of the compressibility effect as we normally know it, this low speed diabatic case should be compared to a transonic (*M*~1) adiabatic case. At *M*=1, the density will be changed by 58% compared that at a stagnation state. We now can have ~60% density change with heat transfer

while still at a low speed (M<0.3) condition. Thus, with the significant heat transfer effect under a thermal boundary condition of a temperature ratio of practical interest (TR=0.62), an aerodynamic flow field at a low-speed condition (M<0.3) flow may no longer be adequately treated as an incompressible flow. The latter flow condition is what is necessarily needed for a linear energy equation and associated passive thermal field as discussed in Section 2. This non-negligible wall heat transfer caused 'compressibility' in an otherwise incompressible flow seems to have been rarely addressed.

3.2 Wall Temperature Dependent Flow Characteristics

3.2.1 General Nonlinear q-Tw Variation and Local HTC

Now we consider the situations where the basic premise for a linear and passive thermal field is neither assured, nor required. Our starting point for the considerations in this context is a high-speed compressible flow. In a compressible flow, the energy equation is fully coupled with the mass and momentum equations. Even for an isothermal case, the q-T_w variation can be a nonlinear curve (Fig. 3-2a), which also covers, as an extreme case, a straight-line variation as in the isothermal incompressible flow case (Fig. 2-1).

With a nonlinear curve, its slope can only be locally measured, equivalent to a local linearization/differentiation of the relevant equations around a base aerothermal state at a given T_w. The differential form of the heat flux variation with wall temperature at any point along the q-T_w curve is:

$$\delta q = \left(\frac{\partial q}{\partial T_w}\right)\delta T_w \qquad (3\text{-}2)$$

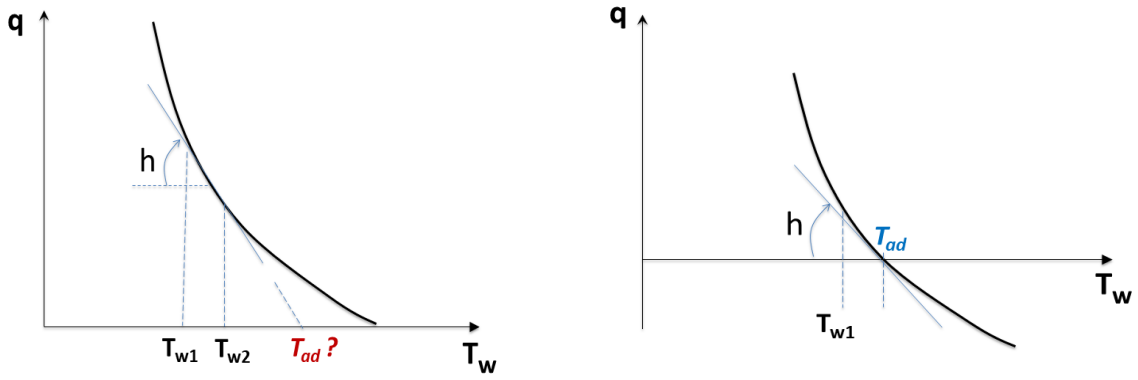

a) Local HTC b) Near-adiabatic HTC & T_{ad}

Figure 3-2 Finite-difference approximation for local HTC for nonlinear q-T_w variation

The slope ($\frac{\partial q}{\partial T_w}$) is effectively the local heat transfer coefficient dependent on T_w. Equation 3-2 can be used as an approximate but consistent way to numerically compute or experimentally measure a local heat transfer coefficient at a given T_w. A finite-difference (FD) approximation of the differential for the local h is (Fig. 3-2a):

$$h = \frac{q_1 - q_2}{T_{w2} - T_{w1}} \tag{3-3}$$

Equation 3-3 is the basis for the two-point method for computing the HTC. The symbols q_1 and q_2 are the heat fluxes calculated or measured at wall temperatures T_{W1} and T_{W2} respectively. The wall temperature difference T_{W2} - T_{W1} should be small enough to reduce the truncational errors of the FD discretization, but also large enough so that the heat flux difference between the two temperature conditions is not drowned in computer rounding errors or experimental noise. For a typical ambient condition, taking 2-3% of inlet flow temperature as the wall temperature difference should be adequate. Note however that although the local HTC is reasonably approximated, the two-point method will not give the adiabatic temperature T_{ad} credibly when the wall temperature is far away from the adiabatic condition and the T_w-q variation is strongly nonlinear as indicated in Fig. 3-2a.

The two-point finite-difference formulation for local HTC provides a consistent and sound basis for heat transfer characterization at a low heat flux condition, even for a nonlinear aerothermal field. Consider a low heat flux condition at T_{w1} close to an adiabatic condition (Fig. 3-2b). Because of the low heat flux magnitude, T_{w1} should be close to the adiabatic wall temperature T_{ad} (Fig. 3-2b). The finite difference for the local HTC may simply be obtained by:

$$h_{ad'} = \frac{q_1}{T_{ad} - T_{w1}} \tag{3-4}$$

where T_{ad} is the fluid temperature at the wall from an adiabatic solution. The two-point method now becomes a one-point method for HTC. Equation 3-4 can be regarded as a one-sided FD approximation for either point 1 of interest, or the adiabatic condition 'ad'. The difference between $h_{ad'}$ and the adiabatic HTC h_{ad} is subject to only truncation errors of the FD approximation. The argument is also applicable to other HT invariant descriptors (the influence coefficients / the discrete form of Green's functions). This is because the heat transfer characteristics in a low flux case can be regarded as linear perturbations around the adiabatic condition. The treatment is consistent with a local linearization around the adiabatic state, thus the aerothermal behaviour should be locally linear - similar to that for the linear energy equation

(discussed in Section 2). The main difference is in the base over which the linearization is carried out. For an incompressible flow, the heat transfer behaviour is linear based on a given flow momentum field which is completely decoupled and solved independently. For a low heat-flux compressible flow state on the other hand, the heat transfer behaviour can be assumed to be locally linear based on a given (and independently solved) adiabatic base flow field.

3.2.2 Aero-thermal Interplay: 'Flow History' Effect and Local Reynolds Number

Now, we shall look at some cases with significant heat transfer influence on the flow at realistic aerothermal conditions. The HTC's dependence on T_w should manifest in terms of how much the heat transfer may change the flow field (which in turn will affect heat transfer) and thus how likely or unlikely a wall-temperature invariant descriptor may be established credibly with adequate accuracy.

Figure 3-3 shows the HTC distributions over a turbine blade surface computed with a RANS model at three different wall cooling conditions of TR = 0.6, 0.75, 0.95 (Maffuli and He [14]). The jump in HTC at a location of 45% surface length on the suction surface is due to the prescribed tripping of laminar to turbulence transition. The impact of the wall thermal condition is relatively small around the leading-edge, but it increases with the streamwise distance. The difference between the coolest wall case (TR = 0.6) and the near adiabatic case is considerable at the trailing edge, up to about 20%. The growing HTC sensitivity along the streamwise surface distance reveals an accumulated 'history effect'. The overall HTC sensitivity to TR consistently indicates that the aerothermal behaviour is in a nonlinear regime, and HTC appears not to be an invariant descriptor even when T_w is at a constant value ('isothermal').

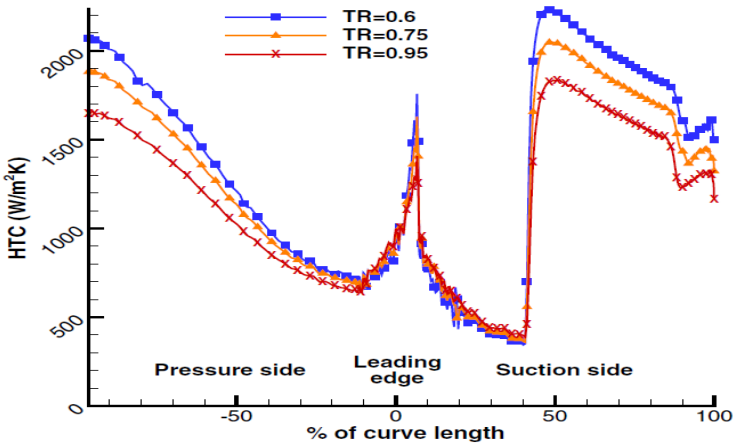

Fig. 3-3 HTC dependence on wall temperature for a turbine blade

(reproduced from *Maffulli & He [14] with permission)*

It is noted that some previous efforts have been made to correct Nu with an exponential form of *TR* (e,g. Fitt et al [15]). The problem is that such correction could only produce a constant correction factor globally for a constant *TR* as in the present case. It thus has no differentiating ability needed for accounting for the history effect as observed, which has to be corrected locally, as highlighted by Maffulli and He [14]. Strong impact of the wall temperature condition on HTC has also been revealed for complex flows around a turbine blade tip, both computationally (Zhang and He [16]) and experimentally (Jiang et al [17]).

Understanding the aerothermal physics for such a history effect can be helped by asking if the flow (momentum) field is indeed altered by the wall heat transfer. To this end, we take a closer look at the velocity profiles across the boundary layer at different locations on the blade (Maffuli and He [14]), as shown in Fig. 3-4.

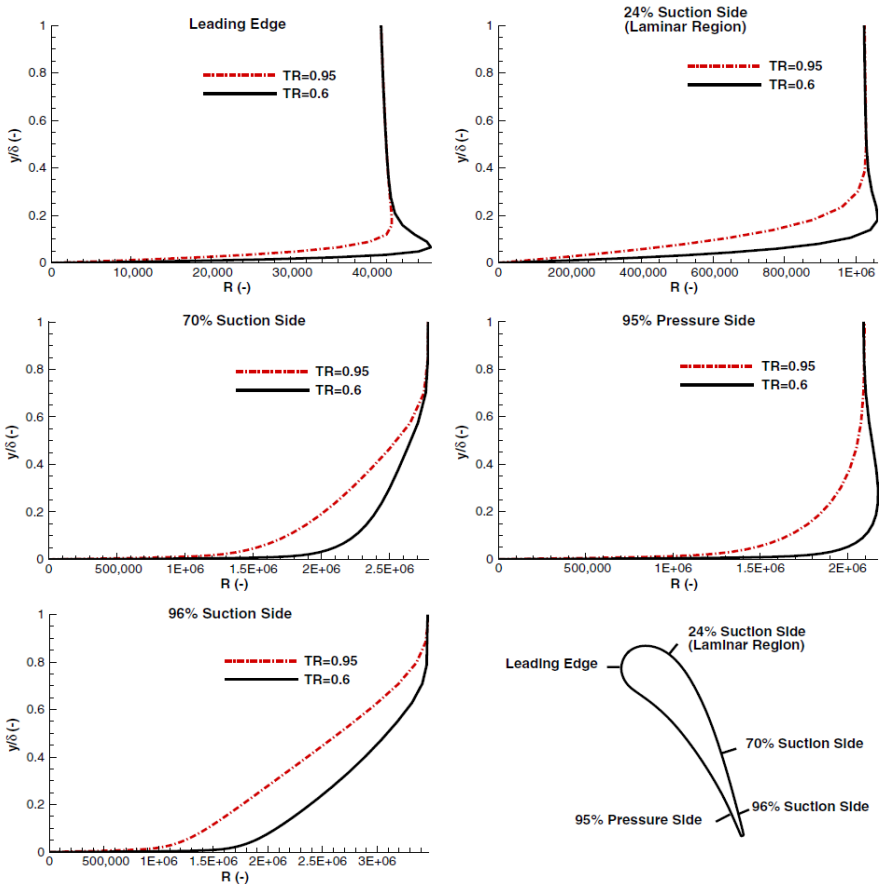

Fig.3-4 Local Reynolds numbers across boundary layer at different surface locations

(reproduced from *Maffulli & He [14] with permission)*

Here the velocity is recast in a non-dimensional form as:

$$R = \frac{\rho V x}{\mu} \tag{3-5}$$

where x is the streamwise distance measured from the leading edge, and thus a constant for each streamwise location. Effectively, *R* is a local Reynolds number, and its change across the boundary layer at different *TR* indicates the impact of wall heat transfer on the flow. The wall cooling (*TR* = 0.6) increases the fluid momentum near wall resulting in a high local Reynolds number with a thinner boundary layer. We can also see that the wall cooling effect grows outwards further downstream and it nearly spans the whole boundary layer at the trailing-edge. Overall, the increased local Reynolds number is consistent with the increased HTC for the cooled wall case (Fig. 3-3). Also, the 'history effect' is shown to be associated with an accumulated upstream influence on the flow field, which is different from the 'history effect' of only changing the fluid temperature field passively advected downstream by a 'fixed' flow field as in an incompressible flow discussed in Section 2.2.

A further test case with a RANS transition model (rather than a fixed transition as in the previous case) interestingly shows an earlier transition for a cooled case as shown in Fig. 3-5 (Maffulli and He [18]). The computed change of the transition with the cooled wall (*TR*=0.6) relative to a less cooled case (TR=0.8) is again in line with the finding that a wall cooling raises the local Reynolds number.

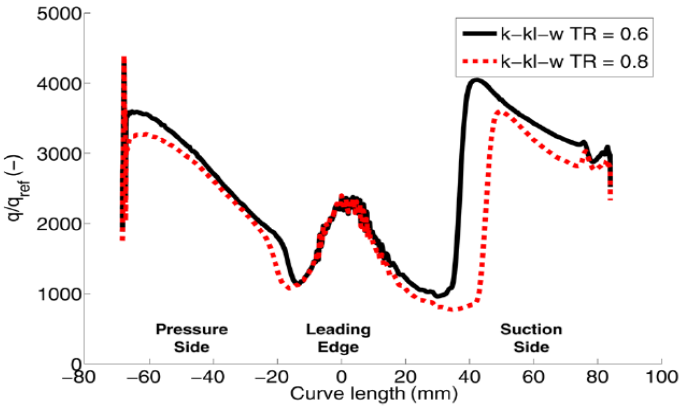

Fig.3-5 Earlier turbulence *transition under a cooler wall (TR=0.6)*

(reprinted from Maffulli & He [18] with permission)

The wall heat transfer effect on the near-wall flow field has been more recently examined with a scale-resolving LES for a surface with micro-structures (Campanaro and He [19]). An array of micro-structures of a semi-spherical shape with radius *r* was subject to an inlet laminar boundary layer of a thickness of 20*r*. The configuration is examined at three wall temperature conditions: cooling (*TR* = 0.5), near-adiabatic (*TR* = 0.98) and heating (*TR* = 1.5). It is observed that wall cooling promotes the laminar-turbulent transition and the heating does the opposite. Figure 3-6

shows the contrast between the near-adiabatic case and the cooled wall case, at the same global Reynolds number, Re_r = 4000 (based on the free stream velocity and the micro-element radius). We can clearly see that while the near adiabatic case is stably laminar (Fig.3-6a); the flow in the cooled wall case already becomes unstable with shed eddies of various sizes and unsteady vortex motion indicating a transition to a turbulent state (Fig.3-6b).

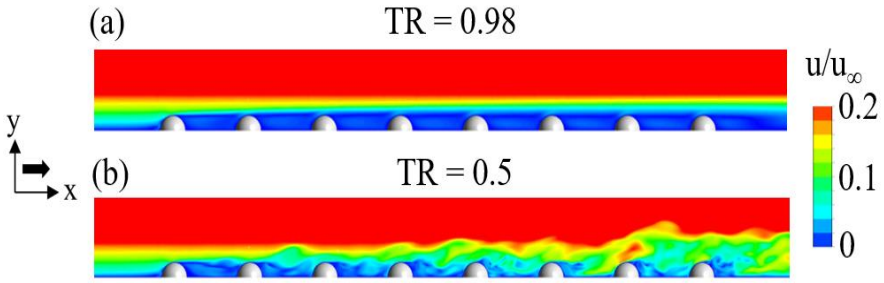

Fig.3-6 Flow fields at Re_r=4000 but two wall thermal conditions (TR=0.5, 0.98)
(reproduced from Campanaro & He [19] with permission)

The computed *Nu* variations with Re_r (Fig. 3-7) give a clear picture about how the performance characteristics around the laminar-turbulent transition can be affected by the wall cooling. The earlier transition for the cooled wall case agrees qualitatively with the increased local Reynolds number as discussed above. The cooling-led earlier transition results in effectively a critical Reynolds number being reduced by ~50%.

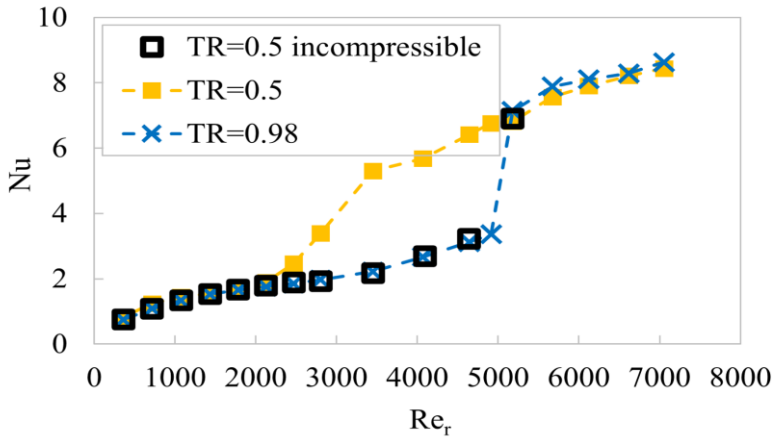

Fig.3-7 *Nu* Variations with Re_r at Two Wall Thermal Conditions (TR=0.5, 0.98)
(reproduced from Campanaro & He [19] with permission)

Also relevant for this low speed flow case (M < 0.3), an additional set of numerical tests is carried out by an incompressible flow model with the fluid properties estimated at the average temperature of the inlet flow and the wall. The incompressible model is indeed shown to fail to predict the difference in the transition between the cooled-wall case and the adiabatic condition, as shown in

Fig. 3-7. The observation also underscores that in an incompressible flow, the energy equation is both linear and passively driven by the flow/momentum field. Therefore, the corresponding thermal field has no feedback/influence on the flow field, as seen here.

It is worth noting that the nonlinear characteristics are mainly confined in the fluid domain, as they should be. Conduction in the solid remains to be essentially linear apart from the temperature dependence of material properties. These nonlinear flow behaviours have significantly increased the motivation for developing and applying fluid-solid coupled solutions.

Overall, we see that for compressible flows, it is difficult to identify a general wall-temperature invariant descriptor for convective heat transfer. The conventional decoupled approach would be further challenged even for an iso-thermal case as already observed. It is noted that there have been many recent efforts in high-fidelity scale-resolving solutions (LES) for convective heat transfer simulations on a fluid-only-domain. These studies have helped develop a fundamental understanding of the impact of turbulence. However, the existence or lack of the heat transfer 'invariant descriptors' should be an importantly relevant consideration. For many conditions and configurations of practical interest, a fluid-solid coupled CHT solution itself may have to be considered as a 'descriptor' (if not the only one) with adequate accuracy for the tasks required.

4. Multiscale Conjugate Heat Transfer

When considering a coupled solution for both the fluid and solid domains together, we need to ask first what key parameters and solution constraints exist for each domain, and what processes occur to communicate between the two domains. The most important aspect is the time scale disparity between the fluid and solid domains and its implications for a coupled conjugate system. In this context, a unified time-dependent solution platform is helpful to facilitate the discussions on both steady and unsteady CHT problems. The time-marching (time-integration) approach which has been extensively adopted for both steady and unsteady flow solutions in the past few decades (e.g. Denton [20], Hah [21], Denton [22], He [23]) is adopted here.

4.1 Time Scale Disparity between Fluid and Solid

Consider a fluid domain of a characteristic length L_f and a solid domain of a characteristic length L_s. Subscripts '*f*' and '*s*' are used to denote the parameters for fluid and solid domains respectively. If the fluid is dominated by convection at a characteristic velocity V_f, the fluid time scale ('throughflow time') is estimated as:

$$\tau_f = \frac{L_f}{V_f} \tag{4-1}$$

For solid conduction, the time scale τ_s can be taken simply by scaling the 1-D unsteady conduction equation, leading to $\tau_s = L_s^2 / \alpha_s$ (for solid thermal diffusivity α_s). The solid conduction time scale is thus,

$$\tau_s = \frac{Cp_s \rho_s L_s^2}{k_s} \tag{4-2}$$

The difference in time scales between two domains can be measured by the ratio:

$$\frac{\tau_s}{\tau_f} = \frac{Cp_s \rho_s L_s^2}{k_s} \frac{V_f}{L_f} \tag{4-3}$$

which can be rearranged as:

$$\frac{\tau_s}{\tau_f} = \left(\frac{Cp_s}{Cp_f}\right)\left(\frac{\rho_s}{\rho_f}\right)\left(\frac{k_f}{k_s}\right)\left(\frac{L_s}{L_f}\right)^2 (Pr_f)(Re_{L_f}) \tag{4-4}$$

For an order of magnitude estimate, take a typical stainless steel as the solid, air at the ambient condition as the fluid, and $L_s = 0.1\, L_f$. We then find:

$$\left(\frac{Cp_s}{Cp_f}\right) \sim O(10^0);\ \left(\frac{\rho_s}{\rho_f}\right) \sim O(10^4);\ \left(\frac{k_f}{k_s}\right) \sim O(10^{-3});\ \left(\frac{L_s}{L_f}\right)^2 \sim O(10^{-2});\ Pr_f \sim O(10^0)$$

The scales then lead to

$$\frac{\tau_s}{\tau_f} \sim O(10^{-1}) Re_{L_f} \tag{4-5a}$$

Thus for a typical Reynolds number of practical interest, Re_{L_f} ~ 10^5, we shall have,

$$\tau_s/\tau_f \sim 10^4 \tag{4-5b}$$

This time scale ratio is similar to the time step ratio between the solid and fluid domains based on the numerical stability and accuracy for the two domains, as estimated by He and Oldfield [24].

The implications of this time scale disparity may be better understood when considering it in conjunction with how a numerical solution method would normally function. A CHT for a fluid-solid coupled domain is an initial and boundary condition problem. For a numerical solution method, its task is to iteratively reduce errors so that a converged solution will satisfy both the discrete equations for all interior mesh points/cells and the boundary conditions on all boundary points (and at fluid-solid interfaces). In the context of a time-marching solution method, all numerical errors will manifest in transient disturbances. The time marching solution can effectively function by driving these numerical transients out of the domains similarly to propagating physical unsteady disturbances, e.g. propagating acoustic/pressure waves upstream

(in a subsonic flow) and downstream at corresponding acoustic velocities, and convecting vorticity and entropy disturbances downstream at local flow velocities.

Computational costs for a converged solution are measured by the number of mesh points in the domains and by the number of time steps needed to drive those numerical error disturbances out of the fluid and solid domains. The number of time steps $N_{\Delta t}$ required is thus influenced by the domain size and the speed at which the transient disturbances are propagated, as well as by the size of the time step Δt. For a fluid domain, major error disturbances tend to be advected at the flow velocity, thus we have $N_{\Delta t_f} = \frac{(L_f/V_f)}{\Delta t_f} = \frac{\tau_f}{\Delta t_f}$. Similarly, for the solid domain, the equivalent error propagation speed is L_s/τ_s for a given domain size and material properties, thus we have $N_{\Delta t_s} = \frac{\tau_s}{\Delta t_s}$.

For steady CHT, the time scale disparity does not make a substantive difference. As both the time scale and the time step size are in proportion for either the fluid or the solid domain, the numbers of time steps for the two domains for a steady CHT are thus comparable to their counterpart for a separate decoupled fluid-only or solid-only solution respectively.

For an unsteady CHT however, there is an acute problem. There are two conflicting requirements that must be satisfied to solve the unsteady CHT problem.

i) The CHT time step needs to be small enough for resolving the smallest disturbance of the coupled domain, which is the fluid unsteadiness in this case. Thus for time-accuracy, we need,

$$\Delta t_{CHT} = \Delta t_f \qquad (4\text{-}6a)$$

ii) The total time scale to be covered needs to be large enough to allow enough time for initial transients and unsteady physical disturbances to propagate through the domain. Otherwise, some boundary conditions are not enacted and the CHT solution will not converge. Thus, for the time-consistence and CHT solution convergence, we need,

$$\tau_{CHT} = \tau_s \qquad (4\text{-}6b)$$

Given the dual requirement of time accuracy and time consistency (Eq. 4-6 a and b), the corresponding number of time steps needed for the unsteady time-domain CHT solution should be,

$$N_{CHT} = \frac{\tau_s}{\Delta t_f} = \frac{\tau_s}{\tau_f} N_{\Delta t_f} \qquad (4\text{-}7)$$

Hence, N_{CHT} can be amplified by a factor ~10^4 times of that for a fluid-only or solid-only solution. Therefore, a direct time-consistent and time-accurate CHT will be prohibitively time consuming and practically infeasible.

It should be noted that there have been various efforts to explore potential options to circumvent or mitigate the challenge arising from the time-scale disparity. The possibility of moderating the time scale disparity with a modified solid material is explored by Diefenthal et al [25], and Łuczynski et al [26], which can lead to some considerable speedup of the transient CHT, but may also be associated to some non-negligible and non-physical fluctuations in the solid, (see Maffulli et al [27]). A hybrid approach is also employed to first use the modified material to provide more rapidly an approximate initial field. Next, a further time marching of the solution with the correct solid material properties (Oh et al [28]) is used to obtain the final results. Alternatively, a hybrid approach can be formulated to solve a steady CHT problem to provide the base steady temperature field, and a time-domain CHT for a fluctuating temperature component in solid domain, marched at a small fluid time step (Koren et al [29]).

Caution should be taken with respect to these hybrid approaches in the context of the time-accuracy and time-consistency (solution convergence) requirements as discussed for Eqs. 4-6 and 4-7. Regardless of how an initial or baseline flow field is obtained, the time domain solution itself is still an initial value problem subject to errors of the initial field. When the solution in the solid domain is marched forward in time in a time-accurate manner, the initial erroneous disturbances will be propagated in the same way as physical unsteady disturbances. Thus, both initial error transients and physical unsteadiness will still have to travel through the whole domain before a converged solution is reached. As such, the time-domain part of the CHT solution will still be subject to the dual time-consistence and time-accuracy requirement and a huge number of time steps will still be required (Eq. 4-7). Otherwise, the accuracy and/or convergence of the time-domain CHT solution will be compromised. In general, the dual time accuracy-consistence requirement in terms of the fluid-resolution and solid-convergence is believed to be the primary challenge in advanced CHT development, particularly for high fidelity scale-resolving turbulent flow solution based CHT methods.

In the following, we will introduce some efforts in developing multiscale methods in order to circumvent this acute challenge arising from time-scale disparity. We will present first a multi-scale time-integration method developed for applications of large scale turbomachinery transient operations and then a Fourier spectral methodology to incorporate a scale-resolving turbulence solver in an efficient and accurate LES-CHT framework.

4.2 Multi-scale Time-stepping for Large-scale Transients

4.2.1 Motivating Considerations: Turbomachinery Transient Operations

The huge time scale disparity seems to provide a natural justification for a fluid-solid scale separation strategy as adopted in the common loosely coupled CHT approach (e.g. Sun et al [30], Errera and Baqué [31]). In a loosely coupled approach for a transient CHT process, the unsteadiness is only retained in the solid domain. The fluid domain is effectively treated as a steady (time-averaged) flow problem and interactions with the solid domain occur in a quasi-steady manner. More specifically, a steady (time-averaged) fluid side will interact with the solid side at each large time step for resolving transient solid conduction. Given that the fluid domain may be subject to a wide range of time-scales within which different time scales may well interact with non-negligible effects, this quasi-steady treatment for the fluid domain may become questionable when there are large-scale low-frequency flow disturbances. Also relevant is when the coupled fluid-solid system is subject to fast transients during a certain part (e.g. a local ramping phase) of an otherwise slow overall process. The recognition of the restrictions of the existing quasi-steady flow assumption for transient CHT has motivated a multiscale time-stepping method (He and Fadl [32]). Here the basic intent is to eliminate the quasi-steady assumption for the fluid domain solution, so that we can include the interactions between short/medium scales and large scales in an efficient manner.

4.2.2 Two-scale Time-stepping for Transient CHT

We start with a scale-dependent flow decomposition,

$$\boldsymbol{U}(x,t) = \tilde{\boldsymbol{U}}(x,t) + U'(x,t) \tag{4-8}$$

Ũ is the flow variable after a low-pass filtering so that it only contains long wavelength disturbances comparable with the large time scales of unsteady conduction in the solid domain, and U' represents the remaining small-scale fluctuations (Fig. 4-1).

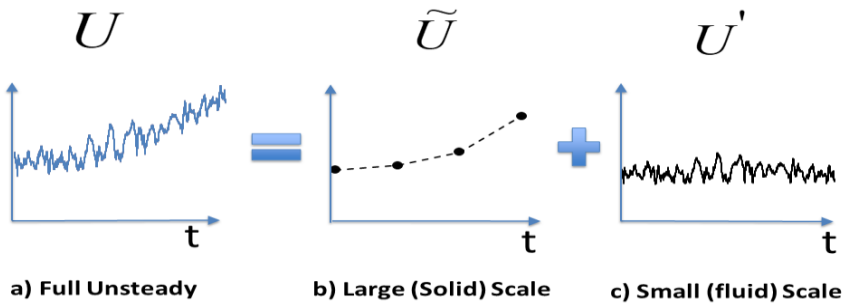

Fig.4-1 Scale-dependent Flow Decomposition

In a discrete time domain, a large-scale time instant t_M is taken corresponding to a solid domain solution. Because of the time-scale disparity, it is assumed that the time-accurate fluid solution would only need to be carried out around a discrete large-scale time instant, as shown in Fig. 4-2. Consequently, for the fluid solution, a small-scale time instant t_n is taken around the large-scale time instant t_M:

$$t = t_M + t_n \tag{4-9}$$

Effectively, the fluid domain is solved in a small time-step on the background of a frozen large-scale temporal variation (Fig. 4-2). A large-scale flow variable is defined by taking a local time-averaging for a sufficiently large number of small time steps N:

$$\widetilde{\boldsymbol{U}} = \frac{1}{N}\sum_{n=1}^{N} U(t_n) \tag{4-10}$$

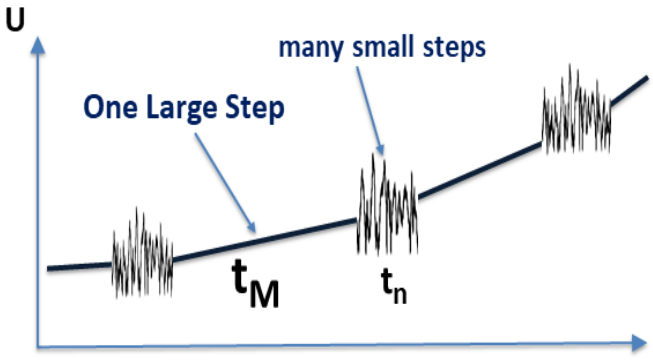

Fig.4-2 Two-scale Time-stepping

The flow governing equations can be expressed in a compact form:

$$\frac{\partial U}{\partial t} + R(U) = 0 \tag{4-11}$$

It can be shown (see He and Fadl [32] for details) that the two-scale fluid equations conditioned by the frozen large-scale time-gradient $(\frac{\partial \tilde{U}}{\partial t})_M$ becomes:

$$(\frac{\partial U}{\partial t})_n + R(U) = -(\frac{\partial \tilde{U}}{\partial t})_M \qquad \text{(n=1, 2, ….., N)} \tag{4-12}$$

It should be remarked that the augmented equations conditioned with the extra source term as expressed in Eq.4-12 is easy to solve with a computational cost comparable to that of a

conventional loosely coupled approach, as demonstrated by He and Fadl [32] and by Fadl and He [33].

The key advantage of the present method is that the quasi-steady assumption is no longer needed. More specifically, for the present multiscale time-stepping CHT method, the source term in the fluid equation (Eq. 4-12) ensures that the whole fluid domain is subject to the influence of the large-scale temporal gradient. In contrast, for a conventional quasi-steady CHT method, the large-scale temporal gradient is completely lost inside the fluid domain, which is only solved subject to the solid wall temperatures at that large-scale time instant, as for a steady flow problem.

Here is an example of a transient natural convection process subject to a fluid boundary ramp-up at different rates (Fadl and He [33]). The fluid-solid coupled domains, computational mesh, and sample results of time-mean and unsteady flow velocities are shown in Fig.4-3.

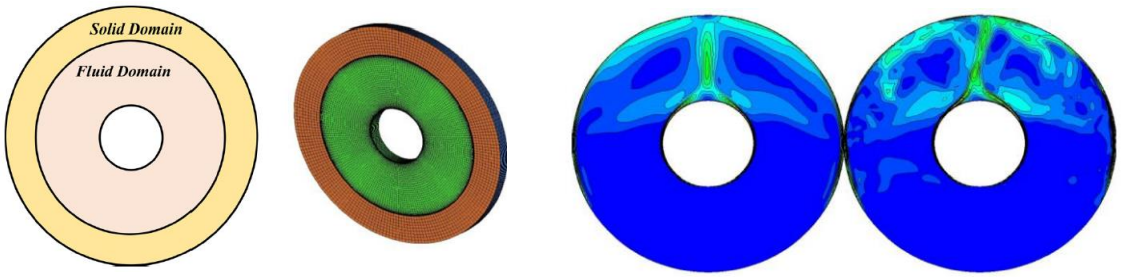

a) Fluid-Solid Configuration b) Time-mean (left) and Unsteady (right) Velocity

Fig.4-3 LES-CHT Case Study for Transient Natural Convection
(reproduced from Fadl and He [33] with permission)

To assess the impact of the conventional quasi-steady assumption, the present unsteady CHT method is also run in a quasi-steady mode by simply switching off the source term in Eq. 4-12. The present multiscale unsteady solution is compared with the quasi-steady one for two cases at different temperature ramping-up rates for the inner wall of the fluid domain. For the slow transient (Fig. 4-4a), the maximum discrepancy in the time averaged temperature on the outer wall surface between the unsteady and quasi-steady model is about 20%. For the fast transient (Fig. 4-4b), the maximum discrepancy rises to 45%. The quasi-steady assumption is clearly not valid in this case. In general, the quasi-steady assumption may not be safe in many seemingly long operations, parts of which consist of relatively short and rapid transients. The present multiscale time-stepping method should provide an effective way to minimize the erroneous

influence of a quasi-steady CHT model on the predicted thermal characteristics of those transient operation processes.

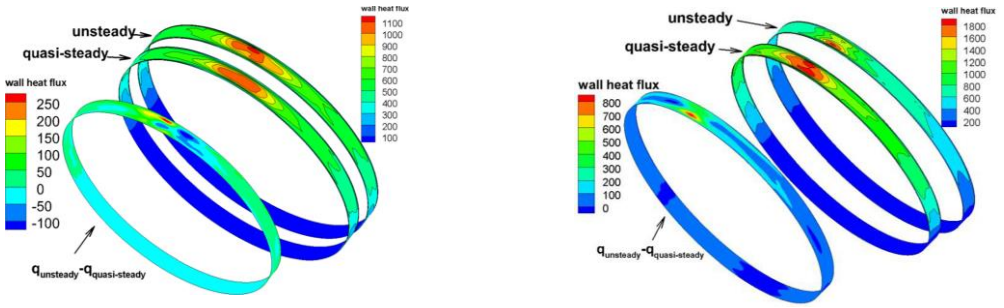

a) Slow Transient (100°K/30s) b) Fast Transient (100°K/1s)

Fig.4-4 Time-averaged Heat Flux at the Fluid-Solid Interface (Unsteady vs. Quasi-steady) (reproduced from Fadl and He [33] with permission)

4.3 Fourier Spectral Methodology for LES-CHT

4.3.1 Motivating Consideration: Wall Temperature Unsteadiness

Consider a fluid-solid coupled system subject to time-invariant steady external boundary conditions. The only source of unsteadiness comes from self-excited flow instabilities, e.g. vortex shedding from a bluff body, or more commonly, flow turbulence. A spatial profile of temperature disturbances around a fluid-solid interface may typically look like that as depicted in Fig. 4-5.

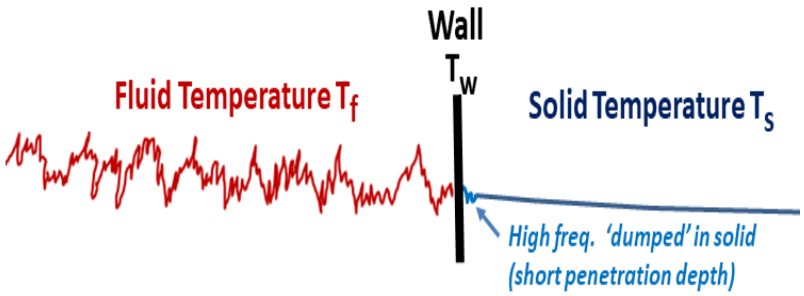

Fig. 4-5 Temperature Fluctuations around the Fluid-Solid Interface

There are two aspects to pay attention to regarding the wall temperature unsteadiness. On the one hand, we should capture its physical impact when it is non-negligible. On the other hand, we

should minimize numerical errors potentially leading to non-negligible spurious wall temperature unsteadiness.

As indicated, temperature disturbances from the fluid side appear to be seemingly ‘dumped’ by solid material with hardly any unsteadiness coming back from the solid to influence the flow. Thus, for the bulk of the solid domain there should be very little unsteadiness in the temperatures. For a homogenous semi-infinite solid domain subject to a thermal temperature impulse on the wall boundary, its penetration depth in solid δ_p depends on the propagation time *t*, as analytically obtained by Faghri et al [34],

$$\delta_p = \sqrt{8\alpha t} \tag{4-13}$$

When the penetration depth for a temperature fluctuation is smaller than the total solid domain size, the unsteady temperature disturbance vanishes in the regions beyond the reach of the penetration. In other words, it does appear that temperature disturbances from fluid get totally ‘dumped’ in the bulk of solid domain beyond the penetration depth. An important question is, what happens to the temperature unsteadiness right on the wall surface? If the wall temperature has non-negligible unsteadiness, the near-wall flow velocities and fluid temperatures may be affected, regardless of how steady the bulk solid domain may be. We should also note the relation between the penetration depth and the wall temperature fluctuations. We may have a very small penetration depth with material of a very low thermal conductivity (e.g. for a wall with Thermal Barrier Coating, TBC). Then we may find a much higher wall temperature fluctuation associated with a much lower wall flux fluctuation, as shown in He [35], Fadl and He [33], and He [36].

A relatively simple option is to filter out all unsteadiness in the fluid domain. Couple a steady or time-averaged flow solution with a steady solid conduction solution (e.g. Sun et al [30], Errera and Baqué, [31], Duchaine et al [37], [38]). However, there is a wide range of self-excited unsteadiness encountered in many practical applications, e.g. from small-scale turbulent eddies in a turbine blade boundary layer to low frequency unstable thermal acoustic modes in combustors. We thus need be able to predict some unsteady CHT characteristics in certain frequency ranges.

Therefore, there is a need for CHT methods to be able to predict unsteady CHT effects in general and the unsteady wall temperature fluctuations in particular, given the wide frequency spectrum of the unsteadiness encountered for various conditions of interest. As discussed earlier, a direct

time-domain CHT solution will be prohibitively costly, so a time-domain CHT methodology in which both fluid and solid domains are time-accurately integrated must be avoided. But is there any possible alternative by which the unsteady CHT effect in terms of wall temperature fluctuations can be predicted adequately at an affordable cost?

A framework for solving the steady and unsteady parts respectively and interactively is envisaged as:

i) to have a baseline CHT method to couple a time-averaged fluid side with a steady solid conduction solution;
ii) to have an unsteady CHT method capable of capturing wall temperature unsteadiness over a wide range of frequencies. However, this unsteady part should not be significantly more costly than that of the baseline steady-like CHT solution.

4.3.2 Discrete Fourier-spectral Representation for Flow Turbulence

The principal pathway taken here is to treat the fluid-solid interface for an unsteady CHT in the frequency domain, rather than in time domain, as instigated by He and Oldfield [24] for deterministic periodic unsteadiness in a temporal Fourier series. The question of interest is, can we use a seemingly deterministic set of harmonics at their corresponding frequencies in a Fourier spectrum to represent seemingly non-deterministic/random turbulence unsteadiness?

In turbulence scale-resolving computations as well as in turbulent flow experiments, turbulence energy is commonly measured using a Fourier spectrum. A time-invariant harmonic in the context of a Fourier spectrum of seemingly 'random' turbulence may simply be interpreted as a statistically mean unsteady component at the frequency captured by Fourier transform over a long enough time period. In this regard it should not be surprising that a discrete Fourier spectrum is used for generating synthetic turbulence fluctuations as an inflow condition for LES, e.g. by Batten et al [39]. There have also been increasing applications of reduced order modelling (ROM) representations of turbulence, e.g. POD (Lumley [40]), DMD (Schmid [41]) and RESOLVENT (McKeon and Sharma [42]). These ROMs are shown to adequately represent the bulk kinematics and dynamics of random turbulence with a relatively small number of deterministic spatiotemporal modes. The successfully widespread applications of ROMs to turbulent flows provide extra support for using a Fourier spectrum in a fluid-solid interface treatment for a scale-resolving LES based CHT method.

We now use a discrete Fourier-spectrum with N_F number of harmonics to approximate a time-varying variable (e.g. temperature T) for a turbulence flow.

$$\mathrm{T}(x,t) = \overline{\mathrm{T}}(x) + Real\left(\sum_{n=1}^{N_F} \widehat{\mathrm{T}}_n e^{in\omega_0 t}\right) \tag{4-14}$$

where the time scale for the Fourier transform is given by the selected low frequency ω_0. For a fluid-solid interface (Fig. 4-6), the fundamental physical condition is the heat flux continuity, as well as the temperatures from both sides to be the same on the wall as T_w.

$$q_f = q_s \tag{4-15}$$

In the Fourier spectral representation, the wall heat flux continuity is formally equivalent to the harmonic balance for each and every harmonic retained in the spectrum.

$$\left(\widehat{q_f}\right)_n = (\widehat{q_s})_n \qquad (n=0, 1, 2, \ldots\ldots, N_F) \tag{4-16}$$

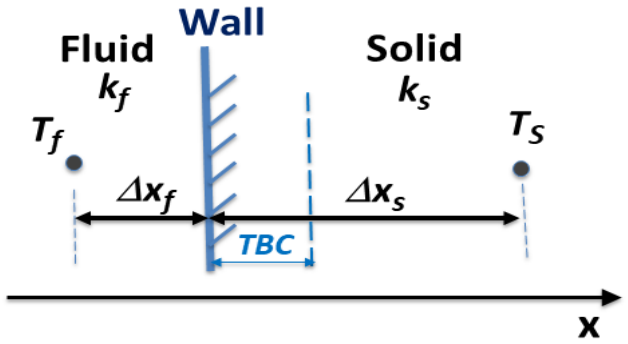

Fig.4-6 Variables at Mesh Points Adjacent to a Fluid-Solid Interface

The framework of the Fourier spectral harmonic balance also provides a consistent basis for treating the steady and time-averaged baseline part of the interface. Consider the harmonic balance for the zeroth harmonic:

$$\left(\widehat{q_f}\right)_0 = (\widehat{q_s})_0 \tag{4-17}$$

It is effectively the balance of the time-averaged fluxes from the fluid and solid sides, thus a manifestation of the physical flux continuity in terms of time-averaged variables. Effectively, the interface can be treated similarly to a steady CHT, once the time-averaged variables for the mesh points adjacent to the fluid-solid interface are available. A moving-average is used to update the time-averaging continuously on-the-fly as the solution proceeds, e.g. for fluid temperature T at the current time step k:

$$\overline{\mathrm{T}}_k = \frac{k-1}{k}\overline{\mathrm{T}}_{k-1} + \frac{1}{k}\mathrm{T}_k \tag{4-18}$$

With the physical temperature continuity at the interface, the time-averaged (the zeroth harmonic) wall temperature is obtained from the fluid and solid temperatures (T_f, T_s) at the mesh points adjacent to the interface (Fig. 4-6):

$$\bar{T}_w = \frac{\left(\frac{\overline{k_f T_f}}{\Delta x_f} + \frac{k_S T_S}{\Delta x_S}\right)}{\left(\frac{\overline{k_f}}{\Delta x_f} + \frac{k_S}{\Delta x_S}\right)} \tag{4-19}$$

It should be noted that Eq. (4-19) only includes the nonlinearity in the time-averaging on the fluid side. For the solid side, the nonlinear effect due to the material property change with temperature is considered to be small, so the zeroth harmonic solid temperature T_s is uncoupled with the solid thermal conductivity k_s during time-averaging. Then, we have the baseline CHT solution established as the zeroth harmonic balance within the Fourier spectral framework.

Now we still need to figure out how the unsteady part for the solid domain can and should be dealt with. A field solution for each harmonic is equivalent to two steady field solutions for the in-phase and out-phase components respectively. If we have to retain a large number of harmonics, for instance, $N_F \sim O(10^2)$, the cost of the temperature harmonic solutions for the solid domain can be very substantial and thus not appealing.

Bear in mind that it is the unsteady temperature at the wall surface which matters as far as the nonlinear fluid side is concerned. In addition, unsteadiness for a large frequency range will disappear in the bulk solid domain because of a limited reach of the corresponding penetration depth as discussed around Eq.4-13. As such, solving harmonics for a wide frequency range in the bulk solid domain will be effectively a waste. What we would like to have is an efficient way to solve the unsteady wall temperatures, preferably without even needing the harmonic temperature field solutions in the solid domain. As to be introduced in the next subsection, such an extremely efficient unsteady CHT interface treatment will be possible with a new semi-analytical harmonic transfer function.

4.3.3 Harmonic Transfer Function for Fluid-Solid Interface

For many years, experimentalists have made extensive use of the transient solid temperature response to a flow impulse disturbance in their transient heat transfer measurements e.g. Schultz and Jones [43], Doorly and Oldfield [44]. For a 1-D semi-infinite solid domain, there is a

complex-number relation between wall heat flux harmonic and wall temperature harmonic for frequency ω:

$$\widehat{q_w} = \widehat{C_{Tq}}\widehat{T_w} \tag{4-20}$$

where the complex number coefficient $\widehat{C_{Tq}}$ is effectively the temperature-heat flux harmonic transfer function for the wall surface. For a single solid domain, we have $\widehat{C_{Tq}} = \sqrt{i\omega}\sqrt{\rho c k}$, where $\rho, c \; and \; k$ are respectively the density, specific heat, and thermal conductivity of the solid. Note that Eq. 4-20 was originally expressed in the Laplace space by Shultz and Jones [43], as used in the transient heat transfer experiments with non-periodic time responses. It was adopted in the frequency-domain with a detailed derivation for single and two-layer solid by He [36] and some validations by He and Oldfield [24].

It should be pointed out that the harmonic transfer function is completely derived from the solid side, reflecting how the wall heat flux and temperature will have to vary in time (harmonically) accordingly for given solid material properties. In the context of unsteady CHT, we would naturally 'constrain' the flux harmonic discretely computed from the fluid side, so that it will follow the same relation because of the physical heat flux continuity in harmonic balance, leading to: $\widehat{q_f} = \widehat{C_{Tq}}\widehat{T_w}$. Next, we use the one-sided finite difference method to approximate the fluid heat flux harmonic $\widehat{q_f}$, leading to a semi-analytical interface condition for the wall temperature harmonic. For a Fourier spectrum of retaining N_F harmonics, the harmonic balance for each wall heat flux harmonic will lead to the following:

$$(\widehat{T_w})_n = (\widehat{TF_w})_n(\widehat{T_f})_n \qquad (n = 1, 2, \ldots\ldots, N_F) \tag{4-21}$$

$$(\widehat{TF_w})_n = \frac{\overline{k_f}}{\overline{k_f} + \Delta x_f \, (\widehat{C_{Tq}})_n} \qquad (n = 1, 2, \ldots\ldots, N_F) \tag{4-22}$$

where $(\widehat{T_f})_n$ is the n^{th} fluid temperature harmonic at the fluid mesh point adjacent to the wall (Fig. 4-6). $\overline{k_f}$ is the time-averaged thermal conductivity at the fluid mesh point. The complex number $(\widehat{TF_w})_n$ is effectively a fluid-solid wall temperature transfer function for the n^{th} harmonic.

The semi-analytical wall temperature transfer function (Eq. 4-22) demonstrates (unexpectedly perhaps) a distinctively useful capability. Now, as long as we have the fluid temperature harmonics at the fluid mesh points adjacent to the wall, we can get the corresponding wall temperature harmonics simply and directly with the wall transfer function $(\widehat{TF_w})_n$. As a result,

we no longer need any unsteady solid field conduction solutions. Consequently, the solid domain can now be solved completely as a steady conduction problem and time-marched with a much larger time-step (by 3-4 orders of magnitude). The steady solid temperatures and the averaged fluid temperature will enable the time-averaged wall temperature to be updated (Eq. 4-19) as the zeroth harmonic baseline CHT interface condition.

For those fluid mesh points adjacent to a solid wall, the fluid temperature harmonics are continuously updated at each time-step with a moving-average discrete Fourier transform (He [36]). In the meantime, the instantaneous wall temperatures are constructed in time with the updated time-averaged wall temperature and updated temporal harmonics. The continuously updated instantaneous wall temperatures will then condition the LES flow solution in time domain.

The extra computational cost for the unsteady part is now only a fraction of that for the baseline steady (time-averaged) CHT solution. This is chiefly because the DFT is only needed on the fluid side of the interface, essentially for one or just few 2-D surfaces in a 3-D fluid domain. The DFT updating is also only needed at each time step (rather than at each sub-iteration). Thus, when we retain as many as $O(10^2)$ harmonics, the extra cost will typically only be ~20-30% of that for the baseline steady (time-averaged) CHT. All considered, we now have a highly efficient unsteady CHT method in which the unsteady part acts more or less like a small add-on part to the baseline steady CHT solution at only a fractional extra computational cost.

4.3.4 Some Computational Examples of Fourier-spectral CHT

A question commonly asked is, when and where should we care about solid wall temperature unsteadiness? From a common fluid flow perspective, one tends to regard most unsteady disturbances at relatively high frequencies as being ‘dumped’ in the solid with hardly any signatures. Hence, we may only need to pay attention to those low frequency dynamics of large magnitude and long penetration into solid domain, e.g. combustor thermal-acoustic modes or circumferential hot streaks through turbines as well as in many other problems of practical interest. An issue of interest but rarely examined is the sensitivity of wall temperature unsteadiness to solid material. It should thus be informative to examine a temperature response of different solid materials to a given fluid incident thermal disturbance of a fixed magnitude at a fixed frequency.

As part of the effort in developing the harmonic interface method (He and Oldfield [24]), the analytical wall heat flux-temperature transfer function (Eq. 4-20) is used as the boundary

condition for a harmonic solution of solid temperature. For a wall subject to a harmonic convective boundary condition with a given heat transfer coefficient *h* and a fluid temperature harmonic of amplitude $\widehat{T_F}$ at frequency *f*, the wall temperature harmonic response (Eq. 4-20) can be rewritten as:

$$\hat{T}_w = \frac{h\widehat{T_F}}{h+\sqrt{i2\pi f}\sqrt{\rho ck}} \tag{4-23}$$

We now use this as the boundary condition for the 1-D conduction in terms of the temperature harmonic in the solid to see how the temperature unsteadiness would behave both at the wall and inside the solid domain. A fluid harmonic temperature disturbance of 10% the value of the reference temperature at a frequency of 1000 Hz and an HTC of 1000 W/m^{2}K are given to represent the fluid side. Three different solid materials are considered: steel, titanium and kapton with their properties shown in Table 1. The computational solid domain length *L* is 0.5 mm, which is longer than the maximum penetration depth estimated. A fine mesh of 1000 mesh points is used to provide mesh-independent solutions.

Table 1 – Thermophysical properties for solid materials

	Steel	**Titanium**	**Kapton**
Density ρ (kg/m^3)	7850	4500	1420
Specific Heat c (J/kg/K)	465	522	1090
Conductivity k (W/m/K)	54	11.4	0.155

The computed temperature amplitude distributions from the wall (*x/L*=0) to the far side with zero temperature harmonic (*x/L*=1) are shown in Fig. 4-7. Regarding the penetration depth, the original expression (Eq. 4-13) is derived for an initial value problem by Faghri et al [34]. Here the flow disturbance is characterised by frequency. We thus use 1/*f* as the time-scale *t*. The corresponding penetration depth can thus be estimated by,

$$\delta_p \approx \sqrt{8\alpha/f} \tag{4-24}$$

As we can see, Kapton has a much more notable local penetration behaviour. A penetration depth of *x/L*=0.0568, estimated from Eq. 4-24, is also marked in Fig. 4-7b. A general observation is that for all cases tested, limited unsteady disturbance penetration into the solid

domain is clearly indicated (Fig. 4-7a) with the computed penetration depths in line with those estimated from Eq. 4-24.

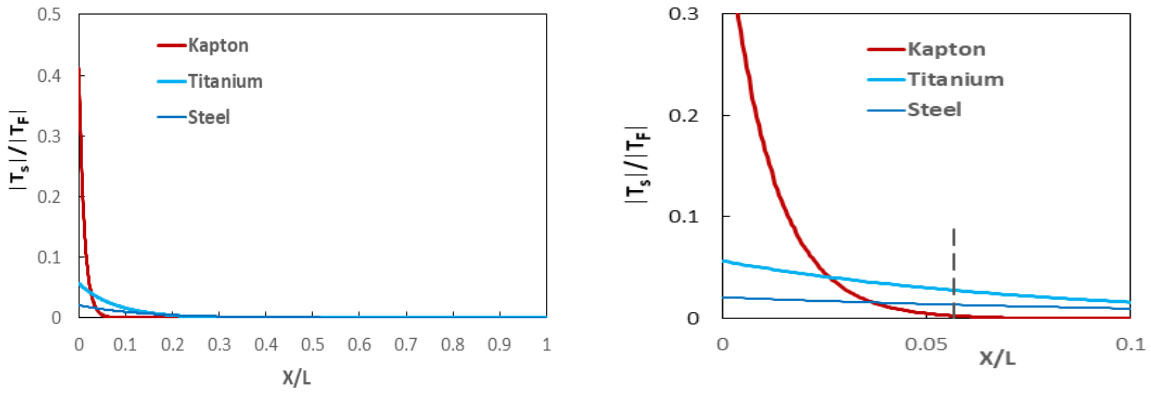

a) Full Domain View (wall at x/L=0)

b) Close-up near the Wall
(Dash line: estimated δ_p/L for Kapton)

Fig.4-7 Penetration of Fluid Temperature Harmonic (T_F) to Solid (L=0.5mm, f=1000Hz)

What is particularly worth noting is that for the material with a low thermal conductivity, the wall penetration decreases and the temperature unsteadiness increases. This is in agreement with the physical consideration of the local energy balance. When the incident heat disturbance can only penetrate into a small volume of solid mass, the local magnitude of the local temperature response will have to increase for the given specific heat capacity. As a result, for the more insulating material, Kapton, the very small penetration leads to a much higher wall temperature response, as high as 40% fluid disturbance in this case. In contrast, for the steel case with high conductivity, although heat disturbance has a much larger penetration into the solid, its wall temperature harmonic response is about 10% of that for Kapton, and only about 0.5% of the incident fluid temperature disturbance. For all three cases, all the incident fluid temperature disturbances get 'dumped' into the bulk solid. But there is a marked difference in wall temperature response among the different materials. Temperature unsteadiness on the wall (rather than in the bulk solid domain) is what is relevant to turbulent flow.

The observed small penetration into only a small fraction of the small solid domain (noting L= 0.5 mm) computed for all three different materials (Fig.4-7) provides a useful context to address another relevant question regarding the validity of the 1D semi-infinite model. The question is in twofold: how one dimensional and how semi-infinite can we treat a typical solid domain boundary in CHT of practical interest?

Consider first the local computational mesh resolution in the wall parallel and the wall normal directions. It is argued that in a wall parallel direction, the mesh spacing will have to be smaller than the smallest turbulent scales resolvable by the fluid mesh. In other words, a local 1D model should be no more restrictive than a local 1D fluid flux evaluation on a boundary face of a fluid mesh cell. The validity of a local 1D model applied to a boundary mesh cell face requires that the penetration in the wall normal direction from this mesh cell face is not impeded by other solid boundary surfaces. This requirement can be adequately satisfied if the penetration depth is comparable to or smaller than the mesh spacing. The question then is, what would the maximum penetration depth be for a typical situation of interest?

Use the original time-domain expression of the penetration depth, $\delta_p = \sqrt{8\alpha\tau}$ (Eq.4-13). For the penetration to reach the solid domain length L_s, the time taken will be comparable to the overall solid time scale τ_S (Eq. 4-2). However, the time scale is now dictated by flow turbulence disturbances, and the longest time period is the throughflow time τ_f (Eq. 4-1). We can see from the discussions in section 4.1 that for a typical aerothermal case of practical interest, we have $\tau_s \sim 10^4\ \tau_f$ (Eq. 4-5b), thus:

$$\delta_{pmax} \sim \sqrt{8\alpha\tau_f} \sim \sqrt{\frac{8\alpha\tau_s}{10^4}} \sim \frac{L_S}{10^2} \qquad (4\text{-}25)$$

Therefore, the maximum penetration depth caused by flow unsteady disturbances shall be in the range of 1% of the solid domain length L_s (thus it is only comparable to a solid mesh spacing). We thus see that the 1D semi-infinite conduction model should be easily justifiable for typical aerothermal problems of interest.

We now turn to a test case of the transonic turbine blade, NASA C3X (Hylton et al [45]). In this case, the main blade passage is subject to an inlet flow stagnation temperature of 800K. The blade is internally cooled at 400K. The solid domain is of nickel steel with the wall surface covered by a TBC layer of 0.1mm Kapton.

We contrast the solutions from two methods. The first method is the present multiscale unsteady CHT method with the Fourier spectral interface treatment. The second is a direct coupling between the LES fluid domain solved at a small fluid time step resolving turbulence eddies and the solid domain solved at a much larger local time-step. This is a typical synchronised but time-inconsistent CHT mode commonly available in commercial codes. It must be pointed out that if the solid conduction is solved in time-domain, the solution convergence can only be expected if the time-integration covers the solid time scale (as discussed in Section 4-1). In such a case, a

time-accurate CHT solution would need to have a prohibitively large number of time steps (by a factor of ~10^4 times, Eq. 4-7) to cover a sufficiently long time period for solution convergence, which would be practically out of reach. The directly coupled but time-inconsistent solution can serve as a useful reference to indicate the level of difference in the unsteady heat transfer results between different CHT coupling methods.

Fig.4-8 shows the cooled turbine blade configuration with the turbulent vortical flow structures downstream of the trailing edge. The time history traces of wall temperature and heat flux are taken from a surface point near the trailing edge, marked as 'A' on Fig.4-8.

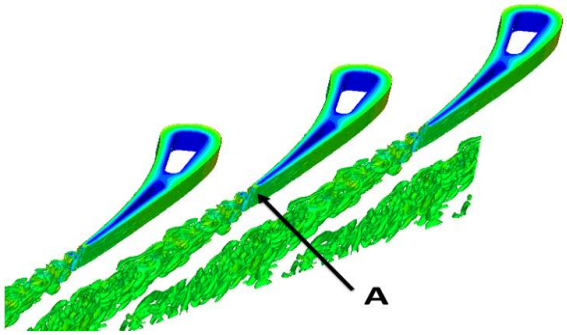

Fig.4-8 Iso-surfaces of vorticity for an internally cooled turbine blade
(reproduced from He [36] with permission),

Figure 4-9 shows the wall temperature variations with time steps for the directly coupled but time-inconsistent solution (Fig. 4-9a) compared with the present Fourier-spectral method (Fig. 4-9b). It is clear that the directly coupled time-inconsistent method overpredicts the wall temperature unsteadiness by about one order of magnitude. Fig. 4-10 presents the corresponding comparison in heat flux between the two methods. We can see that the discrepancies in the calculated wall temperatures also lead to a significant difference in the heat fluxes predicted. In this case, the directly coupled time-inconsistent method (Fig. 4-10a) underpredicts the magnitude of the unsteady heat flux by a factor of 3-5 compared to that of the present Fourier spectral method (Fig. 4-10b).

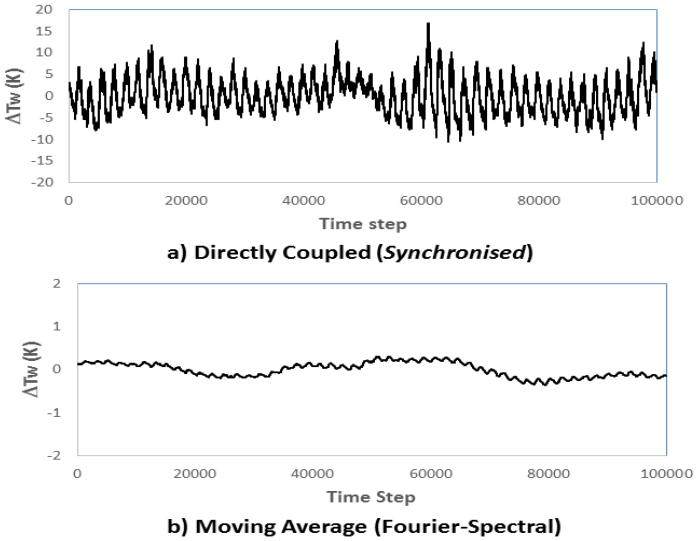

Figure 4-9 Time traces of wall temperature at the blade trailing-edge
(reproduced from He [36] with permission),

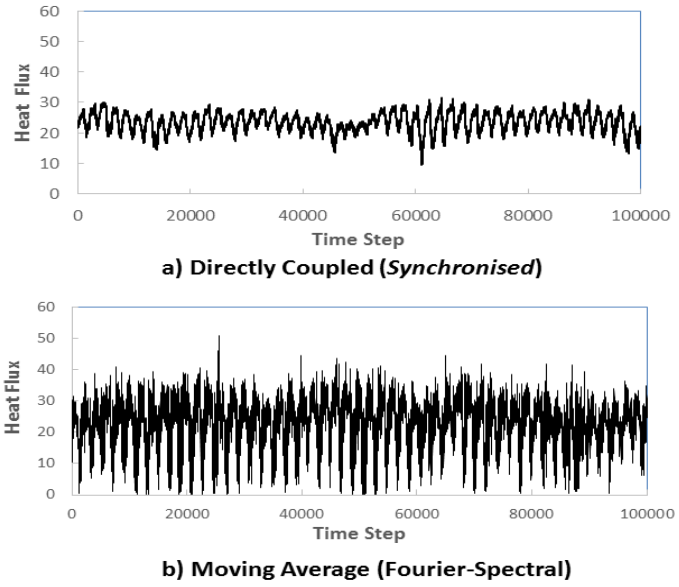

Figure 4-10 Time traces of heat flux at the blade trailing-edge
(reproduced from He [36] with permission),

These result comparisons clearly indicate marked differences due to the wall temperature unsteadiness and how it may be captured accurately and efficiently by a multi-scale Fourier spectral interface method for LES based CHT solutions. Further case studies can be found in He [35] and [36]. Furthermore, for cases with distinctive low frequency disturbances which penetrate through a whole solid domain, a small number of temperature harmonics may be

solved in the solid domain. This capability is demonstrated in a recent extension of the Fourier spectral framework, applied to buoyancy-driven cavity flows by Hickling and He [46]. The LES-CHT results for a cavity flow have also revealed a new type of thermally-driven turbulent flow instability [46], showcasing the potential of LES-CHT development for further applications.

Summary and Concluding Remarks

For fluid-solid coupled conjugate heat transfer (CHT), a general question often raised is why and where it should be needed. The issue is naturally linked to the limit of the conventional fluid-only decoupled approach which seems to have been rarely discussed (somewhat surprisingly). We have learned a few things in addressing the issue.

i) The conventional wisdom of a temperature thermal field completely controlled by fluid mechanics is rooted in an incompressible flow where the energy equation is both linear and decoupled from the mass continuity and momentum equations. Furthermore, only in an isothermal (uniform T_w) condition, can the heat transfer coefficient (HTC) in the exact form of Newton's law of cooling be formally established as a wall temperature invariant descriptor. The latter is needed for a general scaling in conventional convective heat transfer applications.

ii) For non-isothermal cases even in an incompressible flow (thus still subject to a linear and passive thermal field), the heat flux at one wall location will be directly and explicitly dependent on temperatures on all other wall locations. In these cases, the wall temperature invariant descriptors only exist in the form of local wall temperature influence coefficients (the discrete form of Green's functions), whose determination is non-trivial experimentally or computationally. Furthermore, a solid domain (necessarily present for a wall bounded flow) for a non-isothermal case provides extra paths of influence, hence a fluid-domain only setup will, at best, produce an incomplete solution, regardless of the fidelities of flow models and solution methods adopted.

iii) In a compressible flow regime, the energy equation couples with the continuity and momentum, thus the underpinning of a linearly passive thermal field is no longer warranted. It can be shown that for a low speed flow normally deemed 'incompressible', the wall cooling/heating at a realistic temperature ratio (TR) can lead to a significant thermal boundary layer with a level of density changes comparable to that seen in a transonic flow. The impact of wall heat-transfer on the flow field is evident under these conditions, manifested markedly in basic boundary layer flow characteristics including the laminar-turbulent transition. The results consistently

indicate the usefulness of considering a local Reynolds number for such aero-thermal interactive conditions.

Thus, the fluid-solid coupled CHT should have a valuable role to play in both incompressible and compressible flow regimes under many conditions of practical interest. A major challenge in CHT development and application arises from the fluid-solid time-scale disparity. Particularly relevant are time-dependent CHT problems. On the one hand, the time-step needs to be small enough to adequately resolve short and fast unsteady flow disturbances. On the other hand, the time-integration (time-marching) needs to be long enough to propagate transients sufficiently in a slow solid conduction process, otherwise the convergence of an unsteady CHT solution may not be warranted. The constraints imposed by the dual requirement for the time-accuracy and the time-consistency (solution convergence) make a direct time-domain CHT solution prohibitive. Some recent progress in developing accurate and efficient transient CHT methodologies are presented.

i) A multi-scale time stepping for large-scale transient processes, such as those for conventional turbomachinery flexible operations in response to emerging renewable power generations is developed. The new method leads to enhanced solution accuracy by removing the commonly adopted quasi-steady fluid modelling with a new temporal-gradient source term.
ii) A Fourier-spectral framework for scale-resolving turbulence LES based CHT is described. A distinctive semi-analytical fluid-solid temperature harmonic transfer function in conjunction with a moving-average based Fourier transform on the fluid side makes it possible to obtain wall temperature unsteadiness accurately and extremely efficiently. It is shown that the wall temperature unsteadiness can be quite sensitive, numerically to interface methods and physically to solid material. The Fourier spectral LES-CHT methodology enables to capture the wall temperature unsteadiness over a wide range of frequencies, and also serves to make an evidence-based selection of which disturbances should be resolved, when such selection is needed.

Overall, the development of CHT has been part of the continuous pursuit for enhanced understanding and predictability of convective heat transfer. New methods, tools and applications of CHT are and will continue to be developed for existing and new challenges in the field. Clear recognition and comprehensive understanding of the limits of existing methods and approaches should provide further impetus for future development and applications.

References

[1] F. P. Incropera, D. P. Dewitt, T. L. Bergman, A. S. Lavine, Fundamentals of Heat and Mass Transfer, 6th ed, John Wiley & Sons, New York, 2007.

[2] R. J. Moffat, "What's New in Convective Heat Transfer?" Int. J. Heat Fluid Flow, 19(2), pp. 90–101, 1998.

[3] J. Ling, K. J. Ryan, J. Bodart, J. K. Eaton, Analysis of turbulent scalar flux models for a discrete hole film cooling flow, J. Turbomach. 138 (1), 011006. 2016.

[4] P. M. Milani, J. Ling, J. K. Eaton, Generalization of machine-learned turbulent heat flux models applied to film cooling flows. J. Turbomach. 142 (1), 011007, 2020.

[5] J. Hacker, and J. Eaton, Measurements of Heat Transfer in a Separated and Reattaching Flow With Spatially Varying Thermal Boundary Conditions, Int. J. Heat Fluid Flow, 18(1), 1997, pp. 131–141.

[6] J. K. Eaton, "The Discrete Green's Function for Convective Heat Transfer— Part 1: Definition and Physical Understanding,' J. Heat Transfer, 142(1), 102101, 2020.

[7] A. M. Anderson, and R. J. Moffat, "The Adiabatic Heat Transfer Coefficient and the Superposition Kernel Function: Part 1—Data for Arrays of Flatpacks for Different Flow Conditions," ASME J. Electron. Packag., 114(1), 1992, pp. 14–21.

[8] K. A. Batchelder, and J. K. Eaton, "Practical Experience With the Discrete Green's Function Approach to Convective Heat Transfer," J. Heat Transfer, 123(1), 2000, pp. 70–76.

[9] C. W. Booten, and J. K. Eaton, "Discrete Green's Function Measurements in Internal Flows," J. Heat Transfer, 127(7), 2005, pp. 692–69.

[10] D. Mukerji, and J. K. Eaton, "Discrete Green's Function Measurements in a Single Passage Turbine Model," J. Heat Transfer, 127(4), 2005, pp. 366–377.

[11] D.W. Hoffman and J. K. Eaton, Conjugate Heat Transfer Analysis Using the Discrete Green's Function, J. Heat Transfer, 143(2), 2021.

[12] V. Andreoli, D. G. Cuadrado, and G. Paniagua, "Prediction of the Turbine Tip Convective Heat Flux Using Discrete Green's Functions," J. Heat Transfer, 140(7), 2018, p. 071703

[13] J. Saavedra, V. Athmanathan, G. Paniagua, T. Meyer, D. Straub, J. Black, "Scalable Heat Transfer Characterization on Film Cooled Geometries Based on Discrete Green's Functions," Journal of Turbomachinery, 143 (2), 2021.

[14] R. Maffulli, and L. He, Wall Temperature Effects on Heat Transfer Coefficient for High Pressure Turbines. AIAA Journal of Propulsion and Power, 2014, Vol.30, No. 4, pp.1080-1090, 2014.

[15] A. Fitt, C. Forth, B. Robertson and T. Jones, "Temperature Ratio Effects on Compressible Boundary Layers," International Journal of Heat and Mass Transfer, Vol. 29, No. 1, 1986, pp. 159-164.

[16] Q. Zhang, and L. He, Impact of Wall Temperature on Turbine Blade Tip Aero-Thermal

Performance. J. Eng. Gas Turb. and Power, Vol.136, No.5, 052602, 2014.

[17] H. M. Jiang, Q. Zhang, L. He, L. Lu, L. Wang, J. F. Teng, "Experimental Evidence of Temperature Ratio Effect on Turbine Blade Tip Heat Transfer", Journal of Turbomachinery, 140(12), 121010, 2018.

[18] R. Maffulli, and L. He, Impact of Wall Temperature on Heat Transfer Coefficient and Aerodynamics for Three-Dimensional Turbine Blade Passage. J. Thermal Sci. Eng. Appl, Vol. 9, No. 4, 2017.

[19] D. Campanaro, L. He, Impact of Wall Temperature on Aerothermal Characteristics of an Array of Surface Microstructures, Journal of Fluids Engineering, 145(2): 021203, 2023.

[20] J. D. Denton, "A Time Marching Method for Two and Three Dimensional Blade to Blade Flows," ARC R&M 3775, 1975.

[21] C. Hah, "Calculation of three-dimensional viscous flows in turbomachinery with an implicit relaxation method," Journal of Propulsion and Power. Vol. 3, No.5, pp. 415-422, 1987.

[22] J. D. Denton, "The Calculation of Three-dimensional Viscous Flow through Multistage Turbomachine", Journal of Turbomachinery, Vol. 114, No. 1, pp.18-26, 1992.

[23] L. He, New Two-Grid Acceleration Method for Unsteady Navier-Stokes Calculations, AIAA Journal of Propulsion and Power, Vol.9, No.2, pp.272-280, 1993.

[24] L. He, and M. L. G. Oldfield, Unsteady Conjugate Heat Transfer Modelling. Journal of Turbomachinery, Vo1.133, No.3. 2011.

[25] M., Diefenthal, P. Łuczynski, C. Rakut, M. Wirsum, and T. Heuer, 2017, "Thermomechanical Analysis of Transient Temperatures in a Radial Turbine Wheel," ASME J. Turbomach., 139(9), p. 091001.

[26] P. Łuczynski, D. Toebben, M. Wirsum, W. F., Mohr, and K. Helbig, 2019, "Unsteady Conjugate Heat Transfer Investigation of a Multistage Steam Turbine in Warm-Keeping Operation with Hot Air," ASME J. Eng. Gas Turbines Power, 141(1), p. 011005.

[27] R. Maffulli, G. Marinescu and L. He," On the Validity of Scaling Transient Conjugate Heat Transfer Characteristics", Journal of Engineering for Gas Turbines and Power, Vol.142(3), 031021, 2020.

[28] T. K. Oh, D. K. Tafti, and K. Nagendra, Fully Coupled Large Eddy Simulation-Conjugate Heat Transfer Analysis of a Ribbed Cooling Passage Using the Immersed Boundary Method. Journal of Turbomachinery, Vol. 143, Issue 4, 041012, 2021.

[29] C. Koren, R. Vicquelin, and O. Gicquel, Multiphysics Simulation Combining Large-Eddy Simulation, Wall Heat Conduction and Radiative Energy Transfer to Predict Wall Temperature Induced by a Confined Premixed Swirling Flame, Flow, Turbulence and Combustion, Vol.101(1), pp77-108, July 2018.

[30] Z. Sun, J. W. Chew, N. Hills, K. Volkov, and C. Barnes, Efficient Finite Element Analysis/Computational Fluid Dynamics Thermal Coupling for Engineering Applications. Journal of Turbomachinery, Vo1.132, No.3, 2010.

[31] M. Errera, and B. Baqué, A Quasi-dynamic Procedure for Coupled Thermal Simulations. International Journal for Numerical Methods in Fluids, Vol.72, 2013, pp1183-1206.

[32] L. He, L. and M. Fadl, M., "Multi-scale Time Integration for Transient Conjugate Heat Transfer", International Journal for Numerical Methods in Fluids, Vol.83, Issue 12, pp887-904, 2017.

[33] M. Fadl, L. He, On Large Eddy Simulation based Conjugate Heat Transfer Procedure for Transient Natural Convection**.** Journal of Turbomachinery, Vol.139, Issue 11. 2017.

[34] A. Faghri, Y. Zhang, and R.J. Howell, Advanced Heat and Mass Transfer, Global Digital Press, Columbia, MO, 2010.

[35] L. He, Fourier spectral modelling for multi-scale aero-thermal analysis. International Journal of Computational Fluid Dynamics, Vol. 27, No. 2, p118–129, 2013.

[36] L. He, Closely coupled fluid-solid interface method with moving-average for LES based conjugate heat transfer solution. International J of Heat and Fluid Flow, Vol.79, 108440, 2019.

[37] F. Duchaine, Corpron, A., Pons, L., Moureau, V., Nicoud, F., and Poinsot, T., Development and Assessment of a Coupled Strategy for Conjugate Heat Transfer with Large Eddy Simulation: Application to a Cooled Turbine Blade. Int. J. Heat Fluid Flow, 30(6), pp. 1129–1141, 2009.

[38] F. Duchaine, Boileau, M., Sommerer, Y., and Poinsot, T., "Large Eddy Simulation of Flow and Heat Transfer Around Two Square Cylinders in a Tandem Arrangement," J. Heat Transfer, 136(10), 2014, p.101702.

[39] P. Batten, U. Goldberg, and S. Chakravarthy, Interfacing statistical turbulence closures with large-eddy simulation. AIAA Journal Vol.42, No.3, pp485–492, 2004.

[40] J. L. Lumley, Stochastic Tools in Turbulence. Academic Press, New York. 1970.

[41] P. J., Schmid, Dynamic Mode Decomposition of Numerical and Experimental Data. J. Fluid Mech. Vol.656, pp5–28, 2010.

[42] B. J. McKeon, & A.S. Sharma, A critical-layer framework for turbulent pipe flow. J. Fluid Mech. Vol.658, pp.336–382, 2010.

[43] D. L. Schultz, and T. V. Jones, Heat Transfer Measurement in Short Duration Facilities, AGARD AG-165, 1973.

[44] J. E. Doorly, and M.L.G. Oldfield, "The Theory of Advanced MultiLayer Thin Film Heat Transfer Gauges," Int. J. Heat Mass Transfer, Vol.30(6), pp. 1159–1168, 1987.

[45] L.D. Hylton, M.S. Mihelc, E.R., Turner, D.A. Nealy, and R.E. York, "Analytical and Experimental Evaluation of the Heat Transfer Distribution over the Surface of Turbine Vanes," NASA Tech. Rep, CR 168015, 1983.

[46] T. Hickling and L. He, LES-CHT for a Rotating Cavity with Axial Throughflow, Journal of Turbomachinery, Vo1.145, Issue 6, 061006, 2023.